2018

LysMD3 is a type II membrane protein without an in vivo role in the response to a range of pathogens

Christine C. Yokoyama

Megan T. Baldridge

Daisy W. Leung

Guoyan Zhao

Chandni Desai

See next page for additional authors

Authors

Christine C. Yokoyama, Megan T. Baldridge, Daisy W. Leung, Guoyan Zhao, Chandni Desai, Ta-Chiang Liu, Jeremy P. Huynh, Jacqueline M. Kimmey, Camaron R. Hole, Rachel A. Idol, Sunmin Park, Caihong Wang, Ashley Viehmann Milam, Scott A. Handley, Indira U. Mysorekar, Paul M. Allen, Mary C. Dinauer, Tamara L. Doering, Christina L. Stallings, Gaya K. Amarasinghe, Craig A. Micchelli, Herbert W. Virgin, and et al.

LysMD3 is a type II membrane protein without an *in vivo* role in the response to a range of pathogens

Received for publication, December 4, 2017, and in revised form, January 31, 2018 Published, Papers in Press, March 1, 2018, DOI 10.1074/jbc.RA117.001246

Christine C. Yokoyama[a], Megan T. Baldridge[b], Daisy W. Leung[a], Guoyan Zhao[a], Chandni Desai[a], Ta-Chiang Liu[a], Vladimir E. Diaz-Ochoa[c], Jeremy P. Huynh[d], Jacqueline M. Kimmey[d], Erica L. Sennott[e], Camaron R. Hole[d], Rachel A. Idol[f], Sunmin Park[a], Kelly M. Storek[g], Caihong Wang[h], Seungmin Hwang[i], Ashley Viehmann Milam[a], Eric Chen[j], Tobias Kerrinnes[c], Michael N. Starnbach[e], Scott A. Handley[a], Indira U. Mysorekar[a,h], Paul M. Allen[a], Denise M. Monack[k], Mary C. Dinauer[f], Tamara L. Doering[d], Renee M. Tsolis[c], Jonathan E. Dworkin[l1], Christina L. Stallings[d2], Gaya K. Amarasinghe[a], Craig A. Micchelli[m], and Herbert W. Virgin[a3]

From the Departments of [a]Pathology and Immunology and [b]Medicine, Division of Infectious Diseases, and Departments of [d]Molecular Microbiology, [f]Pediatrics, [h]Obstetrics and Gynecology, and [m]Developmental Biology, Washington University School of Medicine, Saint Louis, Missouri 63110, the [c]Department of Medical Microbiology and Immunology, University of California, Davis, California 95161, the [e]Department of Microbiology and Immunobiology, Harvard Medical School, Boston, Massachusetts 02115, the [k]Department of Microbiology and Immunology, Stanford University, Stanford, California 94305, the [i]Department of Pathology, University of Chicago, Chicago, Illinois 60637, the [j]Department of Molecular and Cell Biology, University of California, Berkeley, Berkeley, California 94720, the [l]Department of Microbiology and Immunology, College of Physicians and Surgeons, Columbia University, New York, New York 10032, and [g]Genentech, Inc., South San Francisco, California 95688

Edited by Peter Cresswell

Germline-encoded receptors recognizing common pathogen-associated molecular patterns are a central element of the innate immune system and play an important role in shaping the host response to infection. Many of the innate immune molecules central to these signaling pathways are evolutionarily conserved. LysMD3 is a novel molecule containing a putative peptidoglycan-binding domain that has orthologs in humans, mice, zebrafish, flies, and worms. We found that the lysin motif (LysM) of LysMD3 is likely related to a previously described peptidoglycan-binding LysM found in bacteria. Mouse LysMD3 is a type II integral membrane protein that co-localizes with GM130+ structures, consistent with localization to the Golgi apparatus. We describe here two lines of mLysMD3-deficient mice for *in vivo* characterization of mLysMD3 function. We found that mLysMD3-deficient mice were born at Mendelian ratios and had no obvious pathological abnormalities. They also exhibited no obvious immune response deficiencies in a number of models of infection and inflammation. mLysMD3-deficient mice exhibited no signs of intestinal dysbiosis by 16S analysis or alterations in intestinal gene expression by RNA sequencing. We conclude that mLysMD3 contains a LysM with cytoplasmic orientation, but we were unable to define a physiological role for the molecule *in vivo*.

The innate immune response to infection relies heavily on signals transduced by germline-encoded receptors that recognize common pathogen-associated molecular patterns (PAMPs)[4] such as bacterial and viral proteins, glycoproteins, and microbe-specific nucleic acids (1). These pattern recognition receptors tend to recognize microbial products that are absent in the host, thereby preventing self-reactivity, are often evolutionarily conserved, and may be members of a protein family that recognize similar but distinct microbial products.

Therefore, we were interested in characterizing the evolutionarily-conserved molecule, LysMD3, which has homologs in humans, mice, zebrafish, flies, and worms. LysMD3 is named for its N-terminal lysin motif (LysM) and, in mice and humans, is a member of a protein family that also includes LysMD1, LysMD2, and LysMD4. Recent studies of bacterial and plant LysMs suggest that LysMs bind the glycan backbone of peptidoglycan or the related molecule chitin (2–6). Although peptidoglycan is a ubiquitous bacterial component, relatively little is known about its interactions with the mammalian immune sys-

This work was supported in part by the Children's Discovery Institute of Washington University and St. Louis Children's Hospital (to M. C. D.), Grant 274415 from the Crohn's and Colitis Foundation Genetics Initiative (to H. W. V.), National Science Foundation Fellowships DGE-1143954 (to J. P. H.) and DGE-1143954 (to J. M. K.), and National Institutes of Health Grants T32AI007163 (to C. C. Y.), T32GM007067 (to J. M. K.), T32AI007172 (to C. R. H.), F32AI108089 (to K. M. S.), R01DK100644 (to I. U. M.), R01AI24157 (to P. M. A.), R01AI095396 (to D. M. M.), R01AI102882 (to T. L. D.), and U19AI109725 (to H. W. V.). The authors declare that they have no conflicts of interest with the contents of this article. The content is solely the responsibility of the authors and does not necessarily represent the official views of the National Institutes of Health.

This article contains Figs. S1–S3.

[1] Supported by a Burroughs Wellcome Fund Investigators in the Pathogenesis of Infectious Disease award.

[2] Supported by a Beckman Young Investigator Award from the Arnold and Mabel Beckman Foundation and a Burroughs Wellcome Fund Investigators in the Pathogenesis of Infectious Disease award.

[3] To whom correspondence should be addressed. E-mail: virgin@wustl.edu.

[4] The abbreviations used are: PAMP, pathogen-associated molecular pattern; qRT, quantitative RT; CFU, colony-forming unit; CBP, calmodulin-binding peptide; DPI, days post-infection; MOI, multiplicity of infection; WPI, weeks post-infection; IFN, interferon; HPI, hours post-infection; MEF, mouse embryonic fibroblast; LPS, lipopolysaccharide; UPEC, uropathogenic *E. coli*; PEC, peritoneal exudate cell; TNF, tumor necrosis factor; KO, knockout; RNASeq, RNA sequencing; EGFP, enhanced green fluorescent protein; i.n., intranasally; i.g., intragastrically; i.p., intraperitoneally; LysM, lysin motif; DMEM, Dulbecco's modified Eagle's medium; FBS, fetal bovine serum; BMMo, bone marrow macrophage; UPEC, uropathogenic *E. coli*; IAV, influenza virus; h, human; GT, gene trap; UTI, urinary tract infection.

tem. The intracellular receptors NOD1 and NOD2 have been shown to bind the peptidoglycan fragments Tri-DAP and muramyl-dipeptide, respectively (7), but it is unknown whether the mammalian immune system is capable of recognizing the ubiquitous polymeric glycan backbone of peptidoglycan. Furthermore, a recent study suggested that chitin oligomers may modulate mammalian angiogenesis through interactions with a yet unknown receptor (8). We hypothesized that the LysMD family may represent a novel family of pattern recognition receptors, potentially capable of recognizing important microbial ligands such as peptidoglycan or chitin.

Results from this study revealed that the LysM of LysMD3 is evolutionarily conserved, with orthologs in human, mice, zebrafish, flies, and worms. In mammalian cells, we found that LysMD3 was a type II integral membrane protein that co-localizes with the Golgi marker GM130 with a predicted cytoplasmic location of the LysM. To explore the function of LysMD3 in the immune response, we generated two lines of LysMD3-deficient mice and evaluated the role of LysMD3 in a number of infection and inflammation models. We found no evidence for a role for LysMD3 during the mammalian immune response in the models that we tested, nor did we find a role for LysMD3 in the control of the intestinal microbiota or intestinal gene expression. Additional studies will be required to determine a functional role for this evolutionarily-conserved molecule.

Results

LysMD3 is a predicted transmembrane protein containing an evolutionarily conserved LysM

Mouse LysMD3 (mLysMD3) is a 305-amino acid protein with an annotated N-terminal LysM and C-terminal transmembrane domain (Fig. 1*A*). Phylogenetic analysis of the minimal LysM sequence from multiple model organisms (Fig. 1, *B* and *C*) revealed that mLysMD1, mLysMD2, mLysMD3, and mLysMD4 each clustered with like sequences from other organisms, including *Homo sapiens*, *Xenopus tropicalis*, and *Danio rerio.* Furthermore, groups containing LysMD3 and LysMD4 sequences diverged from clusters containing LysMD1 and LysMD2 LysM sequences. Interestingly, the LysM from *Caenorhabditis elegans* protein F43G9 clustered with LysMD3 and LysMD4 sequences and apart from LysMD1 and LysMD2. Furthermore, whereas the exact relationship between the LysM of mLysMD3 and *Drosophila melanogaster* CG17985 is somewhat less defined, it is apparent that the *D. melanogaster* CG17985 clusters with sequences including mLysMD3/4 and not with mLysMD1/2. The other murine LysM-containing proteins Ncoa7 and Oxr1 cluster separately from CG17985 and the mLysMD family members and are more similar to the *D. melanogaster* protein Mtd (9).

Although there was sequence diversity within LysMs across species, alignment of the deduced proteins demonstrated that several residues were remarkably conserved between prokaryotes and higher order organisms (Fig. 1*B*). In particular, an asparagine residue at position 31 is conserved in all the species analyzed. In addition, amino acids 11–13, with only a few exceptions, were conserved across LysMs from all species analyzed, including several bacterial proteins. A neighboring sequence of amino acids 16–19 had only conservative substitutions across all species.

The mLysMD3 LysM sequence was submitted to the Phyre2 Protein Fold Recognition Server (10) for protein structure prediction. The top hit from this analysis, in which 96% of the sequence was modeled with a confidence of 99.6%, was structure 2djp, a structure of the LysM of human LYSMD1 (data not shown). A model of the mLysMD3 LysM could also be generated based on the structure 2mkx, the LysM from *Enterococcus faecalis* protein AtlA, in which 85% of the sequence could be modeled with a confidence of 99.4% (Fig. 1*D*). Together, these data suggest that the LysM of mLysMD3 and those of mLysMD1, mLysMD2, and mLysMD4 are conserved across multiple divergent species.

LysMD3 co-localizes with GM130+ structures

We next sought to define the subcellular localization of LysMD3. Immunofluorescence staining of endogenous human LYSMD3 (hLYSMD3) in HeLa cells suggested that hLYSMD3 co-localizes with GM130+ structures, consistent with localization to the Golgi (Fig. 2*A*) (11). Importantly, this staining and the co-localization are not observed in HeLa cell lines in which hLYSMD3 expression has been eliminated through the use of CRISPR/Cas9-targeted genome editing. These data are further supported by similar staining patterns using a second commercially-available anti-hLYSMD3 antibody as well as transfection of HeLa cells with an mLysMD3-GFP expression construct (Fig. 2*C*) and subsequent staining for GFP (Fig. S1, *A* and *B*). Additionally, mouse embryonic fibroblast cells (MEFs) were stained for mLysMD3 expression using an affinity-purified polyclonal anti-mLysMD3 antibody raised against amino acids 1–205 of mLysMD3 (Fig. S1*C*). Although this antibody appears to nonspecifically stain the nucleus, LysMD3-specific signals were revealed by the absence of staining in MEFs deficient for m*LysMD3* due to the insertion of a gene-trap cassette downstream of m*LysMD3* exon 1 (Fig. S2*A*). GM130 co-localization was also observed for mLysMD3 in MEFs using this antibody (Fig. S1*C*). Taken together, these data suggest that human and mouse LysMD3 molecules are located on GM130+ structures, consistent with localization to the Golgi.

Pfam analysis of the mLysMD3 amino acid sequence identified a putative transmembrane domain between amino acids 217 and 237 (Fig. 1*A*), suggesting that mLysMD3 is a single pass transmembrane molecule. To test this hypothesis, we first evaluated the cellular compartment with which mLysMD3 is associated. Differential detergent fractionation followed by immunoblotting suggested that mLysMD3 is associated with the membrane compartment of primary bone marrow macrophages (BMMo) and not the nucleus or cytoplasm (Fig. 2*B*). These data are consistent with the hypothesis that mLysMD3 is a transmembrane protein.

We next assessed mLysMD3 membrane topology in a protease protection assay using a recombinant mLysMD3 molecule with N-terminal FLAG and C-terminal HA tags (FLAG-LysMD3-HA, diagrammed in Fig. 2*C*). This construct was expressed in HeLa cells; the plasma membrane was selectively permeabilized using digitonin (12), and exposed epitopes were subjected to proteinase K digestion. Immunoblot analysis of the

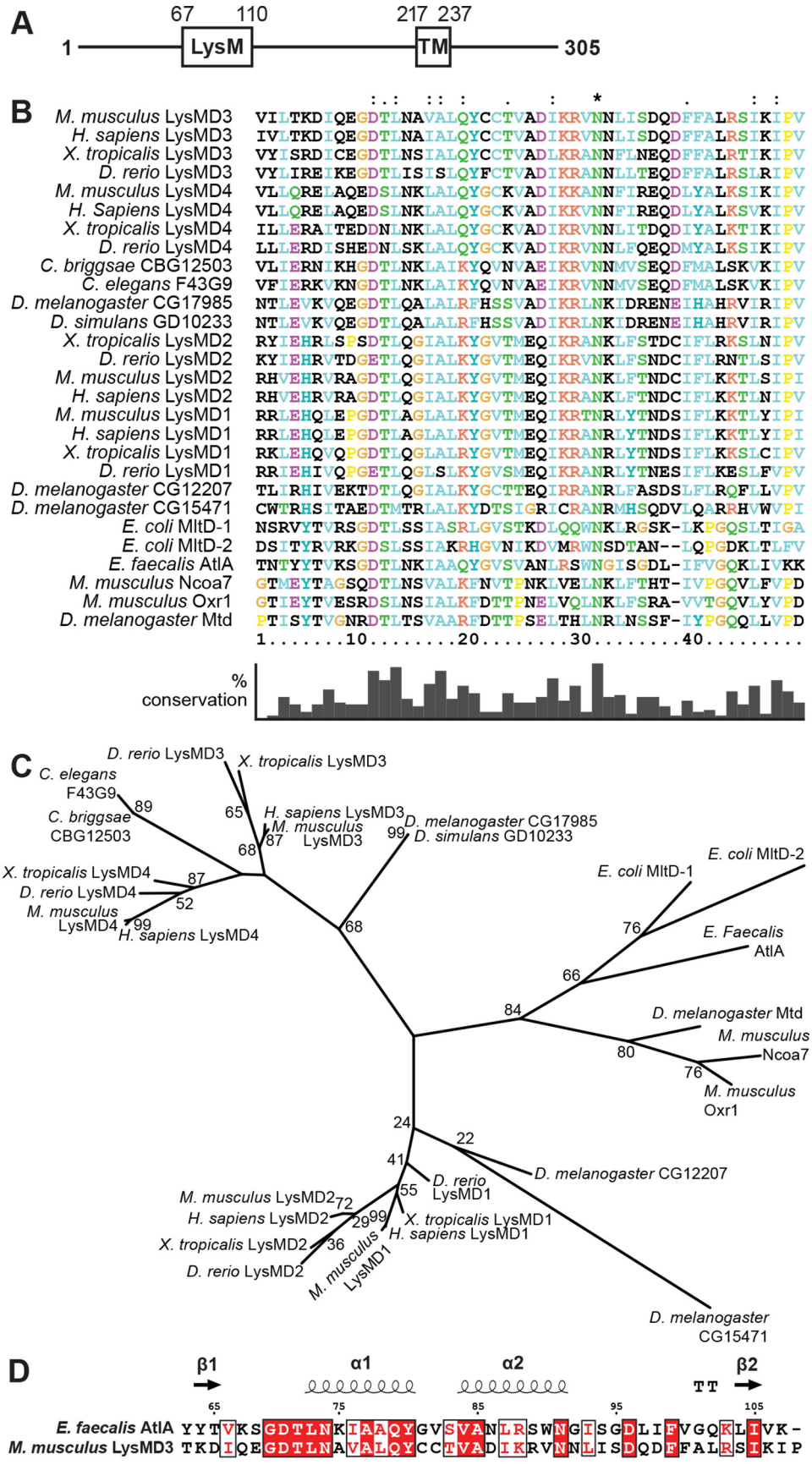

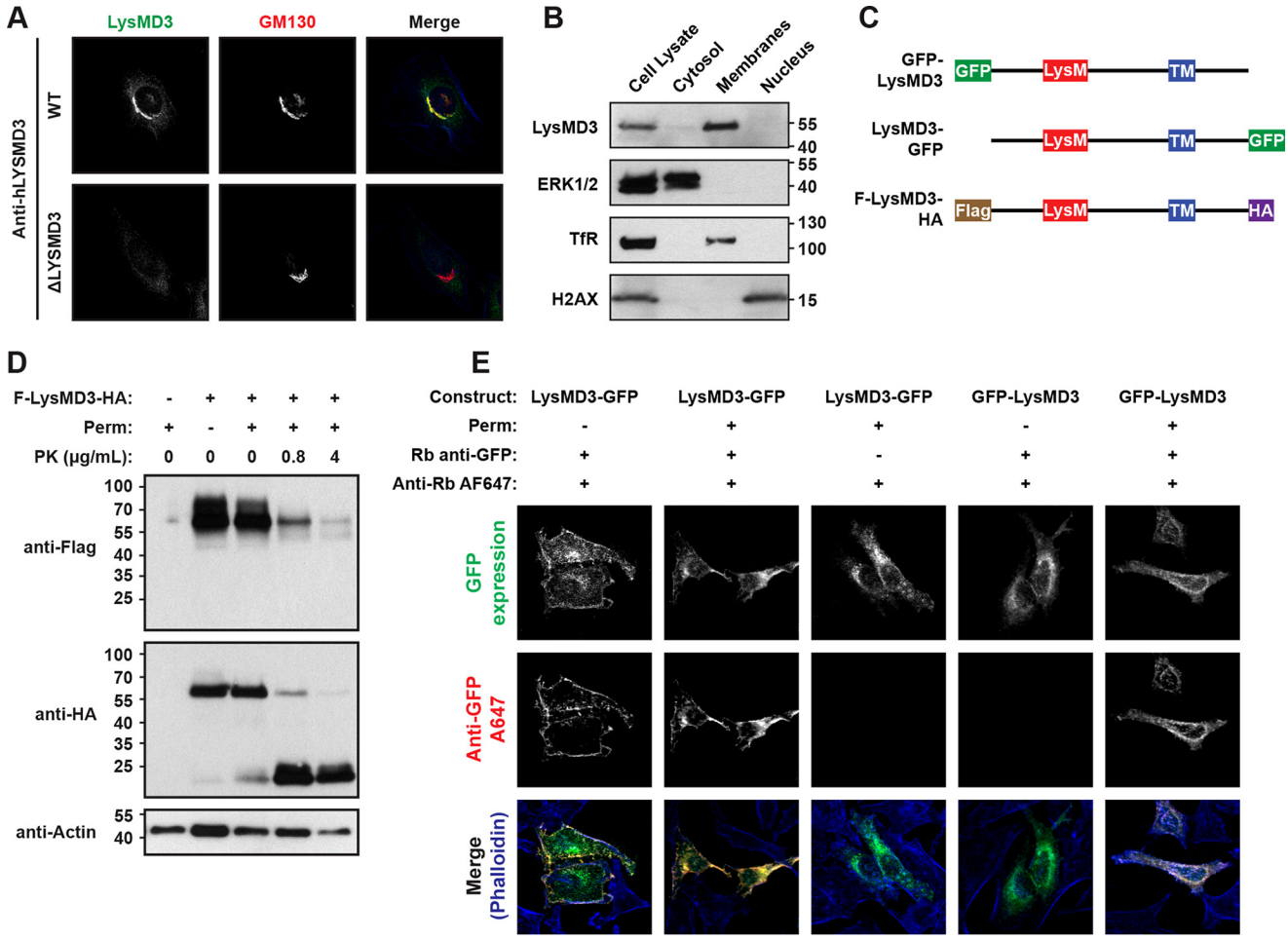

Figure 2. LysMD3 is a type II integral membrane protein that co-localizes with GM130+ structures. *A,* WT and hLYSMD3-deficient ΔLYSMD3 HeLa cells were stained for LysMD3 using a polyclonal anti-hLYSMD3 antibody. Cells were co-stained for GM130, and phalloidin (*blue*) was used to visualize F-actin. *B,* WT BMMo were subjected to differential detergent fraction and immunoblot analysis. Control molecules were ERK1/2 (cytoplasmic fraction), transferrin receptor (*TfR*, membrane fraction), and histone H2AX (nuclear fraction). *C,* diagram of mLysMD3 constructs used in *D* and *E*. *D,* HeLa cells were transfected with a construct expressing FLAG-LysMD3-HA, then permeabilized with Triton X-100, digested with increasing doses of proteinase K, as indicated, and subjected to immunoblot analysis for FLAG, HA, and actin. *E,* HeLa cells were transfected with the indicated constructs. Cells were fixed and stained for GFP ± prior permeabilization with Triton X-100, as indicated. Following GFP staining, all samples were permeabilized, and phalloidin-594 was used to visualize F-actin.

N-terminal FLAG epitope indicated that the FLAG tag was degraded upon permeabilization of the plasma membrane and addition of increasing concentrations of proteinase K, as shown by decreased detection of the FLAG-tagged full-length protein (Fig. 2*D*). In contrast, with increasing concentration of proteinase K, the HA tag was detected on a molecular species that shifted from a molecular mass of about 60 kDa to about 15 kDa, indicating that the C-terminal HA tag was within an intracellular vesicle not permeabilized by digitonin and therefore protected from proteinase K digestion.

This conclusion is further supported by immunofluorescence analysis using GFP-tagged mLysMD3 molecules (diagrammed in Fig. 2*C*). Transfection of HeLa cells with GFP-tagged molecules and anti-GFP staining demonstrated that an mLysMD3 construct with a C-terminal GFP tag could be immunostained at the cell surface without prior membrane permeabilization (Fig. 2*E*). This anti-GFP signal is not observed for an mLysMD3 construct with an N-terminal GFP tag without prior membrane permeabilization.

Overall, these data suggest that mLysMD3 is a type II integral membrane protein located in the Golgi, with the N-terminal LysM located in the cytoplasm.

Generation of LysMD3-deficient mice

To evaluate the role of mLysMD3 during the immune response *in vivo*, we generated a mouse line with gene trap (GT)–mediated disruption of m*LysMD3* using commercially available ES cells. This 129P2Ola/Hsd background cell line con-

Figure 1. Phylogenetic analysis of LysMs. *A,* schematic of predicted domains of mouse LysMD3. *TM*, transmembrane. *B,* multiple sequence alignment of LysMs from the indicated organisms. Positions with a single, fully conserved residue are marked with an *asterisk*. Positions with conservation of residues with strongly similar properties (>0.5 in the Gonnet PAM 250 matrix) or weakly similar properties (≤0.5 in the Gonnet PAM 250 matrix) are marked with a ":" or ".", respectively. Percent conservation of residues is indicated at the *bottom*. *C,* phylogenetic tree of LysMs based on the multiple sequence alignment in *B*. Where known, common protein names are listed. For *E. coli* protein MltD, two LysMs in the protein were evaluated (MltD-1 and MltD-2). *D,* sequence alignment of mLysMD3 and *E. faecalis* AltA. Secondary structural elements from *E. faecalis* AltA (PDB 2KMX) are indicated at the *top*. *T*, hydrogen-bonded turn. The figure was prepared using Espript3.

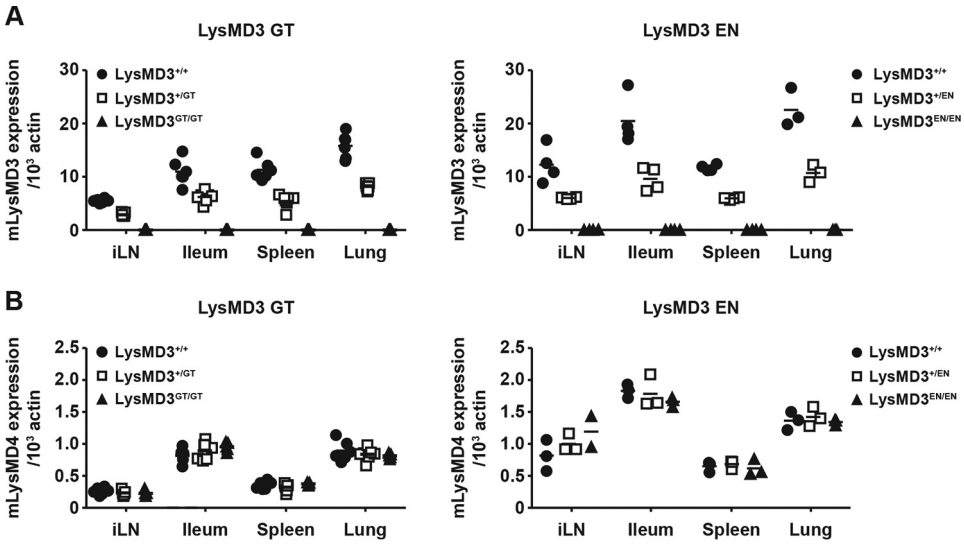

Figure 3. LysMD3-deficient mice lack LysMD3 RNA expression. *A* and *B*, qRT-PCR analysis of LysMD3 (*A*) and LysMD4 (*B*) expression in the indicated tissues from LysMD3 GT and LysMD3 EN mouse lines. All experimental mice were littermate-matched.

tained a β-gal/neomycin resistance GT inserted between exons 1 and 2 of the m*LysMD3* gene, upstream of the protein-coding region (Fig. S2*A*). The location of the GT cassette within m*LysMD3* intron 1 was confirmed by PCR and Sanger sequencing across the cassette and its boundaries (data not shown). The m*LysMD3* GT allele was backcrossed to a C57BL6/J (B6, WT) background with the assistance of microsatellite-based speed congenic analysis at each generation. m$LysMD3^{GT/GT}$ mice were viable and fertile, and crosses of m$LysMD3^{+/GT}$ mice generate offspring with genotypes at the expected Mendelian frequencies on both the 129P2Ola/Hsd and B6 backgrounds.

In knockout (KO) mice generated through gene-trap mutagenesis, it is possible that splicing over the gene trap may occur resulting in expression of the endogenous protein, although often at hypomorphic levels (13). Additionally, it is possible that backcrossing the m*LysMD3* gene-trap allele from one background to another could select for a linked gene with differential immune responses between 129P2Ola/Hsd and B6.

We therefore also generated a KO mouse in which exon 2 of m*LysMD3*, containing the coding region for the LysM, was targeted using CRISPR/Cas9 genome editing in B6 embryos (Fig. S2*B*). Sequencing of the edited m*LysMD3* allele revealed a deletion of ~2 kb, corresponding to the genomic sequence between the guide gRNA sites (Fig. S2*C*). As observed for the mLysMD3 GT mouse line, m$LysMD3^{EN/EN}$ mice are viable and fertile, and crosses of heterozygous parents yield offspring at the expected Mendelian frequencies.

To evaluate expression of m*LysMD3* in our two mouse lines, we used a qRT-PCR assay with primers spanning the exon 2–exon 3 junction of m*LysMD3*. This exon–exon junction was abolished in the LysMD3 EN mouse line and was downstream of the gene-trap cassette in the LysMD3 GT mouse line. In this assay, mLysMD3 transcripts are undetectable in littermates from both lines of mLysMD3-deficient mice (Fig. 3*A*) and are reduced in heterozygous mice, compared with WT.

Genomic alterations have the potential to affect neighboring gene expression (14); therefore, we evaluated the expression of selected m*LysMD3* neighboring genes. We found that expression of *Polr3g* was unchanged in both LysMD3 GT and LysMD3 EN mice (Fig. S2*D*), whereas expression of *Adgrv1* was unchanged in LysMD3 EN mice and was marginally altered in LysMD3 GT mice in a gene-dose–dependent manner (Fig. S2*D*). Finally, given that LysMD3 is a member of a protein family, we evaluated the expression of LysMD4 in the absence of LysMD3. We found that LysMD4 expression was unaltered in both lines of LysMD3-deficient mice in the tissues evaluated (Fig. 3*B*).

These data suggest that alteration of m*LysMD3* has minimal effect on expression of surrounding gene or *LysMD4* expression, and that we have established two lines of mLysMD3-deficient mice, referred to as LysMD3 GT and LysMD3 EN hereinafter.

Lack of a role for mLysMD3 in the response to Citrobacter rodentium and Salmonella typhimurium infection

As our expression data suggested that mLysMD3 is expressed in the intestine, we first evaluated the response of mLysMD3-deficient mice to oral infection with the Gram-negative bacterium *C. rodentium*. In B6 background mice, oral *C. rodentium* infection causes the formation of lesions similar to those caused by the human enteric pathogen enteropathogenic *Escherichia coli* (15, 16). Over the course of infection with *C. rodentium*, minimal morbidity was observed in m*LysMD3* WT or m*LysMD3* KO littermate mice (Fig. 4*A*). Furthermore, no difference in *C. rodentium* fecal shedding was observed over 8 days of infection (Fig. 4*B*). Finally, no difference in colonic inflammation was observed 8 days post-infection (DPI) in the absence of mLysMD3 (Fig. 4, *C* and *D*).

We next evaluated the response of mLysMD3-deficient mice to oral infection with the Gram-negative bacterium *Salmonella enterica* serotype Typhimurium (*S.* Typhimurium). B6 mice are highly susceptible to *S.* Typhimurium infection due to a mutation in *Nramp* (17), but they can be used to model intestinal inflammation during enteric salmonellosis (18). We found that mLysMD3 deficiency did not affect intestinal inflammation after *S.* Typhimurium infection in either the colon or cecum, as

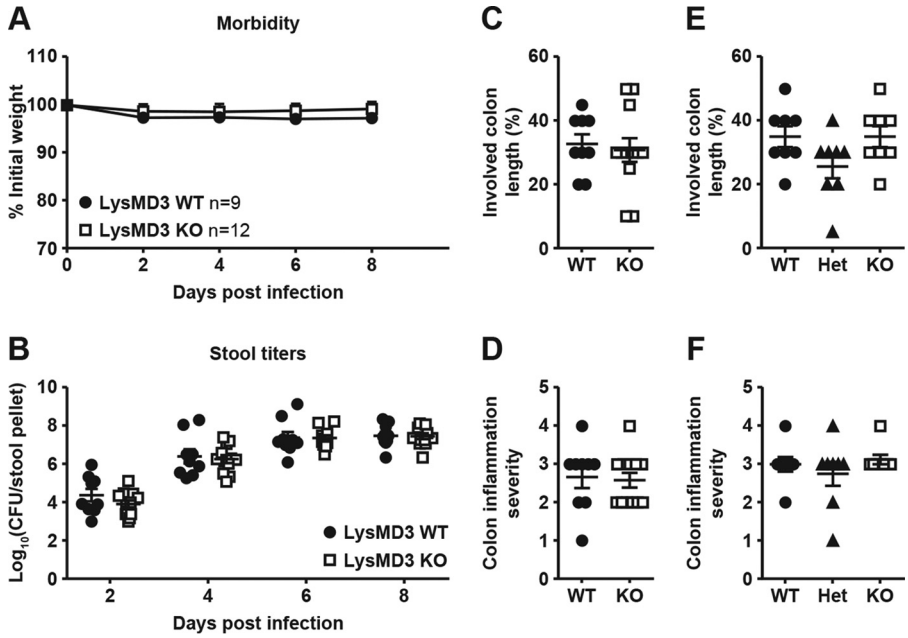

Figure 4. Lack of a role for LysMD3 in the control of *C. rodentium* and *S. typhimurium* infection. Littermate-matched male mice were infected with 1e9 CFU *C. rodentium* on day 0, and morbidity (*A*) and fecal shedding (*B*) were evaluated. At 8 DPI, colons were evaluated for inflammation (*C* and *D*). Each *dot* represents the histology score for one mouse. *E* and *F,* mice were infected with 1e8 CFU *S.* Typhimurium. At 2 DPI, colons were harvested and evaluated for inflammation. All experiments were performed in duplicate using littermate-matched male mice from the LysMD3 EN mouse line.

evaluated by clinical scoring of histological sections at 2 DPI (Fig. 4, *E* and *F* and data not shown).

Lack of a role for mLysMD3 in the response to intracellular bacteria

Given the cytoplasmic orientation of the LysMD3 LysM, we evaluated the role for LysMD3 in the sensing of intracellular bacteria. We evaluated the response of mice to infection with *Listeria monocytogenes*, an intracellular, cytoplasmic Gram-positive bacterium that is a major human pathogen (19). Mice were infected with *L. monocytogenes* and monitored for lethality. We observed no difference in lethality between m*LysMD3* WT and m*LysMD3* KO mice over the course of the experiment, with approximately 50% of each genotype succumbing to infection (Fig. 5*A*). Furthermore, we found no role for m*LysMD3* in the ability of BMMo to activate T cells in response to *L. monocytogenes* infection *in vitro* (Fig. S3*A*).

We next evaluated the ability of mLysMD3-deficient BMMo to respond to infection by a Gram-negative intracellular and cytoplasmic bacterium, *Francisella novicida,* a close relative of the human pathogen *Francisella tularensis*, the causative agent of tularemia (20). Two strains of *F. novicida* were used for these experiments: U112, a WT strain of *F. novicida,* and isogenic mutant Δ*FPI*, which is incapable of escaping the macrophage phagosome to enter the cytoplasm (21). We observed no difference in the ability of either *F. novicida* strain to grow intracellularly (Fig. 5*B*) or to stimulate cell death (Fig. S3*B*) or type I IFN production (Fig. S3*C*) in the absence of mLysMD3. Similarly, no difference in cell death or type I IFN production was seen at a high multiplicity of infection (MOI) of 100 (data not shown).

We next evaluated the ability of mLysMD3-deficient mice to control *Mycobacterium tuberculosis* infection *in vivo* (22–25). *M. tuberculosis* is an intracellular pathogen, classically thought to reside in an early endosomal compartment; however, recent studies have suggested that it may also grow in the cytoplasm (26). We found that there was no overall difference in *M. tuberculosis* titers in the lungs of B6, m$LysMD3^{EN/EN}$, or m$LysMD3^{GT/GT}$ mice at 3 or 13 weeks post-infection (WPI) (Fig. 5, *C* and *D*). Although there was a slight reduction in bacterial titers in the spleens of m$LysMD3^{GT/GT}$ mice at three WPI compared with B6 controls (Fig. S3*D*), this reduction was not observed in m$LysMD3^{EN/EN}$ mice and was not seen at 13 WPI (Fig. S3*E*). Additionally, we did not observe differences in immune cell recruitment to the lung, spleen, or mediastinal lymph nodes of mLysMD3-deficient mice at either 3 or 13 WPI (data not shown).

We next evaluated the ability of mLysMD3-deficient mice to control *Brucella abortus* infection *in vivo*. *Brucella* species cause chronic granulomatous infection in both domestic animals and humans (27, 28). Littermate-matched mice were infected with *B. abortus* intraperitoneally (i.p.), and bacterial titers were determined at 3 DPI. We observed no difference in bacterial titers in the spleen or liver or serum IL6 levels in either LysMD3-deficient mouse line (Fig. 5, *E–G*, and Fig. S3, *F–H*).

We next evaluated the ability of mLysMD3-deficient BMMo to respond to infection with *Legionella pneumophila*, the causative agent of Legionnaire's disease (29). BMMo were infected with *L. pneumophila* strain LP02 or isogenic mutants Δ*flaA* or Δ*dotA*. Δ*flaA* mutants are nonflagellated, nonmotile, and grow to high titers in BMMo, although growth can be restricted by IFNγ priming of BMMo (30). Conversely, Δ*dotA* mutants lack the type IV secretion apparatus that is strictly required for intracellular growth (31). We found no difference in the ability of these bacterial strains to grow intracellularly or to induce cell death in the absence of mLysMD3 (Fig. 5*H* and Fig. S3*I*).

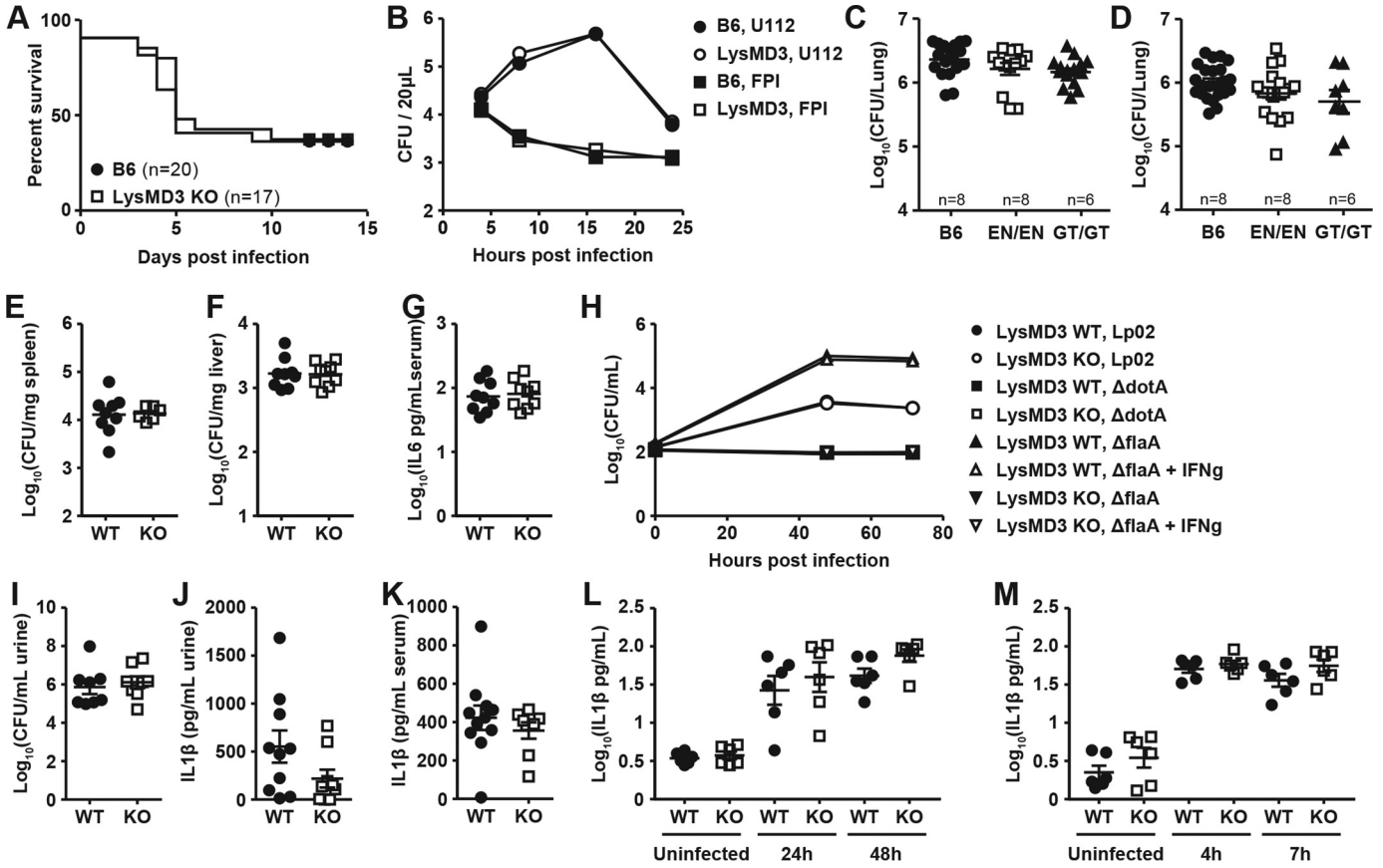

Figure 5. Lack of a role for LysMD3 in the control of multiple bacterial infections. *A,* age-matched mice from the LysMD3 GT mouse line were infected with 5e5 CFU *L. monocytogenes* strain EGD i.p. and monitored for lethality. Data were pooled from three experiments using male mice and one experiment using female mice. Nonlittermate B6 mice were used as controls. *B,* BMMo from the LysMD3 GT mouse line were infected with *F. novicida* strain U112 or isogenic mutant FPI at an m.o.i. of 10, and intracellular growth was evaluated. *C* and *D,* mice were infected by aerosol method with *M. tuberculosis* strain Erdman, and titers in the lungs were determined at 3 (*C*) and 13 (*D*) WPI. *E–G,* mice from the LysMD3 EN mouse line were infected with 1e6 CFU *B. abortus* i.p., and titers in the spleen (*E*) and liver (*F*) and serum IL6 levels (*G*) were determined at 3 DPI. Data were combined from two experimental replicates. *H,* BMMo from the LysMD3 EN mouse line were infected with *L. pneumophila* strains Lp02, ΔdotA, or ΔflaA ± IFNγ, and intracellular growth was evaluated. Data were combined from two experimental replicates. *I–L,* female littermate mice from the LysMD3 GT mouse line were inoculated transurethrally with 1e7 CFU of UPEC strain UTI89. At 24 HPI, urine was collected for CFU enumeration (*I*) and cytokine analysis (*J*), and serum was collected for cytokine analysis (*K*). *L,* MEFs from the LysMD3 GT mouse line were infected with *C. trachomonatis* at an m.o.i. of 10, and levels of secreted IFNb were evaluated by ELISA. *M,* MEFs from the LysMD3 GT mouse line were infected with *S. flexneri* at an m.o.i. of 1, and levels of secreted IFNb were evaluated by ELISA.

We next evaluated a possible role for mLysMD3 in the pathogenesis of urinary tract infections (UTIs) caused by the Gram-negative bacterium uropathogenic *E. coli* (UPEC), which occupies the luminal, intracellular cytoplasmic, and subcellular compartments during infection (32). Mice were transurethrally infected with the clinical UTI isolate, UTI89, and infection as well as the inflammatory response were evaluated 24 h later. We found no difference in urine bacterial titers or urine IL1β production at 24 h post-infection (HPI) in the absence of mLysMD3 (Fig. 5, *I* and *J*). Similarly, there was no difference in serum IL1β production at 24 HPI (Fig. 5*K*). Histological evaluation of bladders from UPEC-infected mice demonstrated no role for mLysMD3 in the severity of inflammation at 24 HPI (Fig. S3*J*). We also evaluated the ability of mLysMD3-deficient BMMo to respond to UPEC infection *in vitro*. We found there was no difference in IL1β production by mLysMD3-deficient BMMo at either 6 or 24 HPI (Fig. S3*K*).

Finally, we evaluated the ability of mLysMD3-deficient MEFs to respond to infection by clinically relevant intracellular bacteria species *Chlamydia trachomatis* and *Shigella flexneri*. We saw no difference between LysMD3 WT and KO cell lines in production of IFNβ in response to *C. trachomatis* (Fig. 5*L*) or *S. flexneri* (Fig. 5*M*). Similarly, no difference was seen in the production of IL6 in response to infection (Fig. S3, *L* and *M*).

Lack of a role for mLysMD3 in models of inflammation

Datasets from the Immunological Genome Project (Immgen) (33) suggest that mLysMD3 transcripts are expressed in cells of the immune system, as well as in intestinal tissues that could likely come into contact with pathogens. Therefore, we next evaluated a number of additional models of inflammation and infection.

Immgen datasets suggest that LysMD3 transcripts are highly expressed in neutrophils (33). Therefore, we hypothesized that mLysMD3 could regulate inflammation in the neutrophil-dependent KRN model of serum-induced arthritis (34, 35). Mice were intravenously injected with arthritogenic serum from KxB/N mice on day 0 and monitored for disease progression. In littermate-matched male mice, we found that there was no difference in arthritis induction, as assessed by weight loss (Fig. 6*A*), ankle swelling (Fig. 6*B*), and clinical scoring (data not shown) up to 7 days post-serum transfer. Furthermore, there

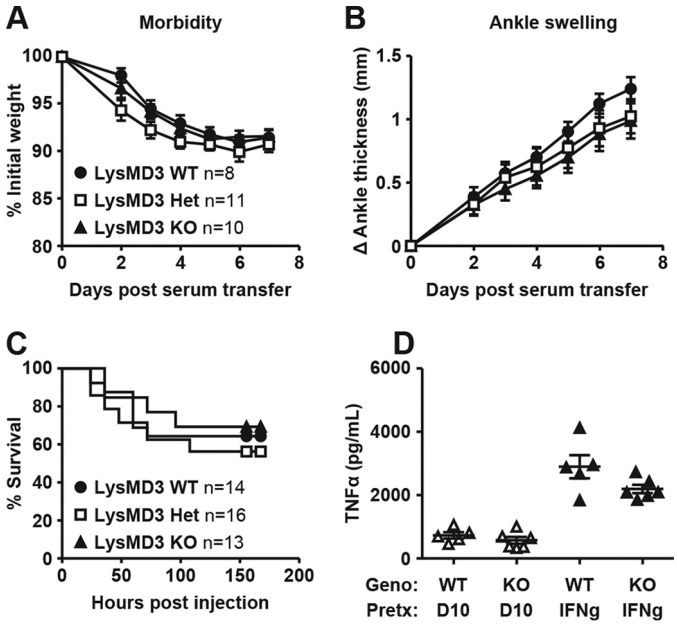

Figure 6. Lack of a role for LysMD3 in mouse models of inflammation. Mice were i.v. injected with KBN serum at day 0 and monitored for weight loss (*A*) and ankle swelling (*B*). Data were pooled from two experimental replicates using littermate male mice from the LysMD3 EN mouse line. *C,* mice were injected i.p. with 20 mg/kg LPS and monitored for death every 12 h. Data were pooled from three experimental replicates using littermate-matched female mice from the LysMD3 GT mouse line on a mixed B6/129P2Ola/Hsd background. *D,* PECs from the littermate-matched LysMD3 EN mouse line were stimulated with 10 ng/ml LPS ± IFNγ pretreatment. At 6 h post-stimulation, TNFα levels were measured in the supernatant fluids by ELISA. Data were pooled from two separate experimental replicates.

were no observable histological differences in the affected joints at that time point (data not shown). Separate experiments with nonlittermate-matched mice suggested that resolution of swelling after arthritis induction was similarly unaffected by mLysMD3 deficiency (data not shown).

We next tested whether mLysMD3 played a role in the inflammatory response to bacterial products. To address this, we challenged mice with lipopolysaccharide (LPS) and monitored them for mortality (Fig. 6*C*). We found there was no difference in LPS-induced death in the absence of mLysMD3. Similarly, we found that peritoneal exudate cells (PECs) from littermate-matched mLysMD3-deficient mice produced similar levels of pro-inflammatory cytokines after *ex vivo* stimulation with LPS (Fig. 6*D*).

Lack of a role for mLysMD3 in response to viral infection

Given that mLysMD3 is highly expressed in the lung (Fig. 3*A*), we tested whether mLysMD3 played a role during respiratory viral infection. We first evaluated the ability of mLysMD3 to control influenza virus (IAV) infection *in vivo*. Mice were infected with mouse-adapted influenza virus H1N1 strain PR8 intranasally (i.n.) and monitored for morbidity and mortality. We found no difference in the susceptibility of mLysMD3-deficient mice to infection with IAV PR8 over the course of the experiment (Fig. 7*A*).

We also evaluated the role of mLysMD3 in the control of herpesvirus reactivation from latency. Mice were latently infected with the γ-herpesvirus MHV68 and the ability of MHV68 to reactivate from PECs was evaluated (36, 37). We found no difference in viral reactivation from latently infected LysMD3 WT or LysMD3-deficient PECs (Fig. 7, *B* and *C*).

Lack of a role for mLysMD3 in response to fungal infection

Given that LysM domains have been found capable of binding to chitin (5, 38), we evaluated the role of mLysMD3 in the host response to fungal infection. Mice were infected with *Cryptococcus neoformans* strain KN99α and monitored for lethality (Fig. 8*A*). In one of three experiments, LysMD3 KO mice were significantly more resistant to *C. neoformans* infection than their WT littermates. However, this finding was not replicated in two subsequent experiments. We also found no role for mLysMD3 in the response to *Aspergillus fumigatus* infection *in vivo*. Mice were infected with *A. fumigatus* i.n. and monitored for morbidity. We observed no difference in weight loss over the course of the experiment, and we saw no difference in cell recruitment to the lung at 4 DPI (Fig. 8, *B* and *C*). Evaluation of lung tissue from *A. fumigatus*-infected mice revealed no difference in lung inflammation or fungal hyphae growth in the absence of mLysMD3 (data not shown).

Lack of a role for mLysMD3 in controlling intestinal bacterial populations or intestinal gene expression

Interactions between host and pathogen are likely to be distinct from interactions between host and commensal organisms. Given that publicly available datasets (39) and our own analysis (Fig. 3*A*) suggest that LysMD3 was expressed in the intestine, we assessed whether mLysMD3 regulated host interactions with the commensal microbiota. To test this hypothesis, we co-housed littermate WT and mLysMD3-deficient mice for 2 weeks to homogenize the microbiota between mice and to correct for variability due to differences in breeding cohorts. Mice were then singly housed for 2 weeks on a regimen of broad spectrum antibiotics in Kool Aid or Kool Aid alone. Fecal pellets were collected for 16S analysis, and ileal tissue samples were prepared for RNASeq. We found no difference between WT and mLysMD3-deficient mice in bacterial richness or diversity within treatment groups in either mLysMD3-deficient mouse line (Fig. 9, *A* and *B*). We did observe a significant drop in richness and diversity in the antibiotic-treated groups, as expected (Fig. 9, *A* and *B*). We also applied principal component analysis to these datasets and found that although there was a clear difference between Kool Aid-treated and antibiotic-treated mice, there was not a distinct separation of mice by genotype (Fig. 9*C*). Finally, RNASeq analysis of ileum samples from both the mLysMD3 GT and LysMD3 EN lines demonstrated no differentially expressed genes between WT and mLysMD3-deficient mice with or without antibiotic treatment that reached significance in both mouse lines (Fig. 9*D*).

Lack of a role for mLysMD3 in the innate immune response to C. rodentium infection

Finally, we tested whether mLysMD3 played a role in the innate immune response to infection, which may have been obscured by the presence of the adaptive immune system in previous experiments. To address this possibility, we crossed the LysMD3 EN mouse line to the Rag1 KO background (40). Littermate-matched LysMD3 WT and KO mice on the Rag1

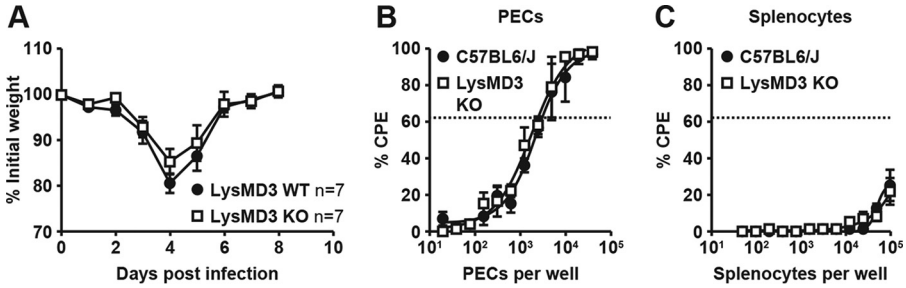

Figure 7. Lack of a role for mLysMD3 in the control of influenza and gHV68 viral infection. *A,* mice were anesthetized and infected IN with H1N1 strain PR8 and monitored for weight loss. Data were pooled from two experiments using littermate-matched female mice from the LysMD3 EN line. *B* and *C*, mice were infected with MHV68 i.p. At 16 DPI, PECs (*B*) and splenocytes (*C*) were harvested, serially diluted, and plated on a monolayer of MEFs. At 3 weeks post-harvest, MEF monolayers were scored for cytopathic effect, indicating the present of latent virions. Data were pooled from three experiments using nonlittermate B6 mice as a control and the LysMD3 GT mouse line.

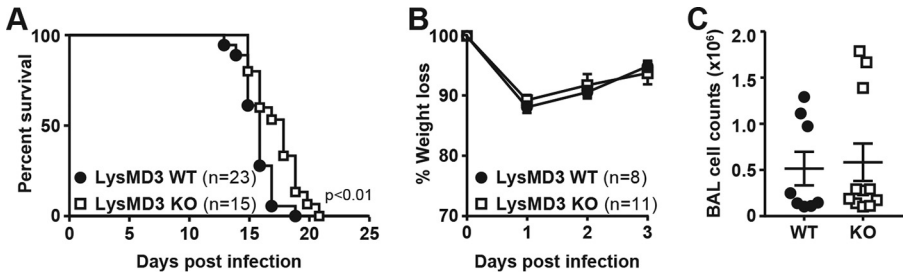

Figure 8. Lack of a role for mLysMD3 in the response to *C. neoformans* and *A. fumigatus* infection. *A,* mice were infected i.n. with 5e4 CFU of *C. neoformans* and monitored for lethality. Aggregated results from three independent experiments are shown. Mice were sacrificed if the body weight dropped below 80% of initial starting weight. *B* and *C*, mice were infected i.n. with 1e7 *A. fumigatus* conidia and monitored for weight loss (*B*). At 4 DPI, lungs were lavaged, and BAL cell counts were determined (*C*).

KO background were infected with *C. rodentium* and monitored for lethality. We found no difference in lethality (Fig. 10*A*) or stool titers (Fig. 10*B*) over the course of *C. rodentium* infection.

Discussion

The annotated LysM domain of mLysMD3 is evolutionarily related to similar domains in human, frog, and zebrafish with orthologs in flies and worms. We found that mouse and human LysMD3 proteins co-localize with GM130+ structures and that they are type II integral membrane proteins, with the LysM domain with a cytoplasmic orientation. In extensive studies of two independent lines of mLysMD3-deficient mice, we observed no evidence for a physiological role for this molecule in a range of pathogen infections, models of inflammation, or interactions with commensal bacterial. One explanation for these *in vivo* findings is that, while evolutionarily conserved, mLysMD3 has no physiological role. Alternatively, we simply failed to select the right model in which to detect a phenotype for mLysMD3 deficiency, or there is redundancy that obscures the function of this conserved molecule. The latter hypothesis is supported by the lack of an observable developmental phenotype in our mLysMD3-deficient mice.

Significance of mLysMD3 localization and immune functions of endoplasmic reticulum and Golgi proteins

We originally hypothesized that mLysMD3 was a candidate pattern recognition receptor due to homology between the LysMs in flies and plants. Furthermore, publicly available databases and datasets (39, 41, 42), as well as our own data, suggest that mLysMD3 is expressed in tissues where it could feasibly be involved in the sensing of invading pathogens or interactions with the commensal microbiota. Interestingly, however, we found that mLysMD3 co-localizes with GM130+ structures in human and mouse cells, consistent with localization to the Golgi (11), and furthermore, mLysMD3 is a type II integral membrane protein with LysM in the cytoplasm. Although traditional paradigms for PAMP-sensing focus on localization of pattern recognition receptors at the cell surface, it is now appreciated that intracellular organelles such as mitochondria, the endoplasmic reticulum, and the Golgi apparatus can serve innate immune signaling platforms (43). For instance, in primary cells isolated from *Drosophila* infected with *Wolbachia pipientis* bacteria, *Wolbachia* can be identified in a GM130+ cellular compartment or an immediately adjacent compartment (44). In mammals, *S.* Typhimurium establishes the *Salmonella*-containing vacuole near the Golgi apparatus (45). Furthermore, *Salmonella enterica, B. abortus, C. trachomatis,* and *L. pneumophila* have all been shown to co-opt intracellular trafficking and redirect Golgi-derived vesicles during infection (46). However, we were unable to define a role for mLysMD3 in models of these infections and multiple others. Furthermore, we found that mLysMD3-deficient mice have no evidence of dysbiosis or altered intestinal gene expression. It remains possible that mLysMD3 interacts specifically with a particular microbial product or ligand that we did not evaluate in our studies.

Evolutionary conservation

Despite the fact that mLysMD3 appears to be evolutionarily conserved with proteins found in flies, zebrafish, and worms, it is possible that its function is not conserved. Although *Toll* and

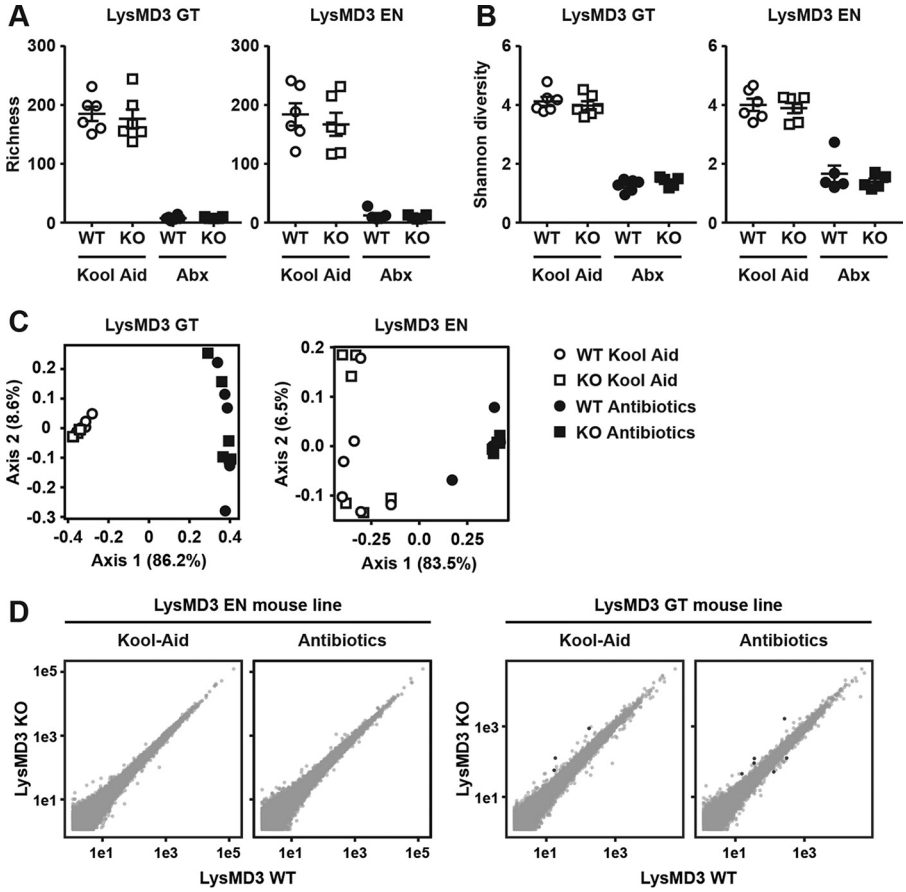

Figure 9. No microbiota or gene expression alterations in intestines of LysMD3-deficient mice. Littermate-matched WT and LysMD3-deficient (*KO*) mice from both mouse lines were co-housed for 2 weeks, then subjected to 2 weeks of oral broad-spectrum antibiotics in Kool Aid, or Kool Aid alone. Post-treatment fecal samples were subjected to 16S rRNA sequencing, and ileal RNA was subjected to RNA-Seq analysis. Based on 16S sequencing, bacterial species richness (*A*) and α diversity (*B*) were evaluated. *C,* principal component analysis was applied to weighted UniFrac distances based on 16S rRNA sequences. *D,* average expression values were calculated for each gene across replicates and plotted on a log10 scale by genotype. Genes with average expression values of <10 were omitted. Genes with at least 2-fold change in expression with adjusted *p* values of <0.1 appear as *black* with the remainder in *gray*. There were no genes with adjusted *p* values of <0.01.

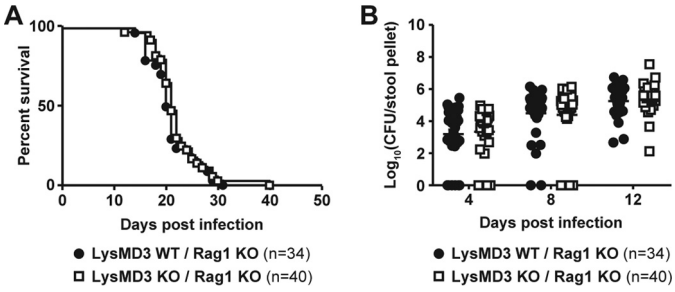

Figure 10. Lack of a role for LysMD3 in the innate immune response to *C. rodentium* infection. The LysMD3 EN mouse line was crossed onto the Rag1 KO background. Littermate mice were infected with 1e9 CFU *C. rodentium* i.g. Lethality (*A*) and *C. rodentium* fecal shedding (*B*) were monitored.

Toll-like receptor family members are central to immune responses in flies and mammals (47, 48), the evolutionarily-conserved peptidoglycan recognition proteins (PGRP and PGLYRP), while essential for the *Drosophila* immune response, to date have been found to play a relatively minor role in mammalian immunity (49, 50). It is possible that LysMD3 is conserved for reasons completely unrelated to a role in immunity, despite its defining peptidoglycan-binding lysin motif, such as a role during organismal development. Indeed, the *Drosophila* molecule *Toll* plays an important role in dorsal-ventral polarity during embryogenesis (51), with secondary function as an important element of the immune response in adult flies (48, 52). Furthermore, LysMD family member expression in zebrafish has been shown to be up-regulated during embryogenesis, with localization to the central nervous system, but without alterations in expression in response to bacterial challenge (53).

mLysMD3 redundancy

LysMD3 is a member of a protein family, and LysMD4 is predicted to also contain a LysM and a transmembrane domain. It is possible that mLysMD4 may compensate for mLysMD3 deficiency in our mouse lines. However, we saw no evidence of mLysMD4 transcript up-regulation in mLysMD3-deficient mice, although it is possible that compensation may occur at the level of protein regulation or in the context of physiological levels of expression. It is also possible that the more distantly related family members mLysMD1 and mLysMD2 could compensate for mLysMD3 deficiency. However, obscuring of mLysMD3 function by mLysMD1 or mLysMD2 redundancy seems unlikely, given that the evolutionary distance between these molecules is significant (Fig. 1*C*), and mLysMD1 and mLysMD2 are not predicted to be membrane-bound proteins.

Table 1
Primers and gRNA

Target	Primer sequence
mLysMD3 GT genotyping A	GAGCCCCCAAATGAAAGAC
mLysMD3 GT genotyping B	GTCTAGACCGGGTGGATGAA
mLysMD3 GT genotyping C	TCTTCGCGCATCTGTCTCTA
mLysMD3 EN genotyping A	TACAACAGGGTCTCAACCACG
mLysMD3 EN genotyping B	GCTGGCAGCAAGAACCTTTG
mLysMD3 EN genotyping C	AGGTCACCAGTAAAGGAATTTCA
Mouse actin qPCR F	GCTCCTTCGTTGCCGGTCCA
Mouse actin qPCR R	TTGCACATGCCGGAGCCGTT
Mouse actin qPCR probe	CACCAGTTCGCCATGGATGACGA
mLysMD3 EN gRNA 1	GCCAGAGACACCCCGATACCTGG
mLysMD3 EN gRNA 2	GCTTTGTAACCTGCCCGATAGGG
hLysMD3 gRNA	TGACCACTTGACTGAACTCCNGG

Mice deficient for multiple family members will be required to evaluate a role for the LysMD protein family in mammalian biology.

Materials and methods

Mice

The embryonic stem cell line Lysmd3Gt(E201G10)Wrst (clone E201G10, 129P2Ola/Hsd background) was purchased from the German Gene Trap Consortium. A single male chimeric founder was bred to B6 mice and backcrossed to >99% B6J background with high-density (~10 centimorgans) microsatellite–marker-based speed congenic analysis at each generation with the assistance of the Speed Congenics Facility of the Rheumatic Diseases Core Center at Washington University School of Medicine. LysMD3 gene trap mutant mice were genotyped using primers listed in Table 1, with GT mutant alleles identified by primers A + C and WT alleles identified by primers B + C. To generate CRISPR/Cas9-modified mLysMD3-deficient mice, B6 embryos were microinjected with mLysMD3 EN gRNA 1 and 2 (Table 1) and Cas9 mRNA and transferred to pseudopregnant recipient female mice, as described previously (54). Mice were screened for loss of exon 2 by Southern blotting, and targeted alleles were verified by Sanger sequencing. A single male founder was crossed to a B6 female, and F1 pups were intercrossed to generate subsequent breeding pairs and experimental animals. Mice were genotyped using the primers listed in Table 1, with WT alleles identified by primers A + B and EN mutant alleles identified by primers A + C. All mice were bred and housed in an enhanced barrier-specific pathogen-free facility at Washington University in St. Louis. All experiments were performed using age- and sex-matched mice between 8 and 12 weeks of age generated by intercrossing heterozygous mice (littermate mice), unless otherwise noted. *B. abortus* experiments were performed at the University of California Davis using age- and sex-matched littermate mice between 7 and 17 weeks of age. Experiments conducted at Washington University were approved by the Institutional Animal Care and Use Committee of Washington University. *B. abortus* experiments conducted at the University of California Davis were approved by the University of California Davis Institutional Animal Care and Use Committee.

Cell culture

MEFs were established from embryos derived from progeny of an LysMD3 GT heterozygous mouse cross, genotyped as above, and used before passage six. Unless otherwise stated, MEFs derived from WT littermates were used as controls. MEFs were grown in DMEM supplemented with 10% (v/v) FBS and 1% penicillin/streptomycin. All HeLa cell lines were maintained in DMEM with 10% FBS. h*LYSMD3* HeLa KO cells (ΔLYSMD3) were generated using CRISPR/Cas9 genome editing at the Genome Engineering and iPSC Center at Washington University School of Medicine (St. Louis, MO), as described previously (55). Briefly, h*LYSMD3* exon 2 was targeted using hLysMD3 gRNA (Table 1), and single cell clones were sequenced to confirm the complete absence of WT alleles and disruption of the ORF.

Plasmids

To generate an N-terminal FLAG and C-terminal HA expression vector, the Gateway cloning vector pTAG-attR-C1 (56), containing three N-terminal FLAG/CBP tags, was modified to encode three in-frame HA tags downstream of the Gateway cloning site. To generate an insert tagged with an N-terminal EGFP, the FLAG/CBP motif in pTAG-attR-C1 was replaced with EGFP. The cDNA IMAGE clone 3156298 containing mLysMD3 was purchased from ATCC. The mLysMD3 protein-coding region was PCR-amplified and cloned into the Gateway destination vectors described above. mLysMD3 was also cloned into pEGFP-N1 (Clontech) using Gibson assembly master mix (New England Biolabs). All expression plasmids were sequence-verified.

Antibodies

Rabbit polyclonal anti-LysMD3 antibody was raised against amino acids 1–205 of mouse LysMD3 (Cocalico). mLysMD3(1–205) was conjugated to AffiGel15 (Bio-Rad) and used to affinity-purify the resulting immune serum. Commercially available antibodies were as follows: anti-β-actin (Sigma A5316); anti-ERK1/2 (Cell Signaling 4695); anti-FLAG M2 (Sigma F1804); anti-GFP (Abcam ab6556); anti-GM130 (Pharmingen 610822); anti-H2AX (Millipore 07-627); anti-HA (Sigma H9658); anti-hLysMD3 (Sigma HPA018024 and Proteintech 24313-1-AP); and anti-transferrin receptor (Life Technologies, Inc., 13-6800). Secondary antibodies were as follows: donkey anti-rabbit AF488 (Invitrogen A21206); goat anti-mouse AF555 (Invitrogen A21425); goat anti-mouse AF633 (Invitrogen A21052); donkey anti-rabbit AF647 (Invitrogen A-31573); goat anti-mouse HRP (Jackson ImmunoResearch 115-035-146); and goat anti-rabbit HRP (Jackson ImmunoResearch 111-035-003).

Phylogenetic analysis

Phylogenetic analysis was performed using the maximum likelihood method in the MEGA6 package (57) with 500 bootstrap replicates. The tree with the highest log likelihood is shown. Phylogenetic trees were visualized using TreeView (58). Sequences used for the phylogenetic analysis were as follows: *Caenorhabditis briggsae* CBG12503, XP_002640031; *C. elegans* F43G9, NP_001122475; *D. melanogaster* CG12207, NP_650352; *D. melanogaster* CG15471, NP_572187; *D. melanogaster* CG17985, NP_610305; *D. melanogaster* Mtd, NP_652017; *D. rerio* LysMD1, NP_001070218; *D. rerio*

LysMD2, NP_001003507; *D. rerio* LysMD3, NP_001002104; *D. rerio* LysMD4, NP_957144; *Drosophila simulans* GD10233, XP_002080462; *E. coli* MltD-1, NP_414747; *E. coli* MltD-2, NP_414747; *E. faecalis* AtlA, NP_814543; *H. sapiens* LysMD1, NP_997716; *H. sapiens* LysMD2, NP_699205; *H. sapiens* LysMD3, NP_938014; *H. sapiens* LysMD4, AAH84545; *M. musculus* LysMD1, NP_694761; *M. musculus* LysMD2, NP_081585; *M. musculus* LysMD3, NP_084533; *M. musculus* LysMD4, NP_780424; *M. musculus* Ncoa7, NP_766083; *M. musculus* Oxr1, NP_001123635; *X. tropicalis* LysMD1, NP_001096341; *X. tropicalis* LysMD2, NP_001037868; *X. tropicalis* LysMD3, NP_001017308; and *X. tropicalis* LysMD4, XP_012815036.

Cell fractionation and immunoblot

WT bone marrow macrophages were generated as described previously (59). Briefly, bone marrow cells were cultured in 10% FBS, 10% CMG14-12 supernatant fluids containing macrophage colony-stimulating factor (60). At day 7, cells were subjected to differential detergent fractionation using a QProteome kit (Qiagen), according to the manufacturer's instructions. Fractions were subjected to Western blot analysis with antibodies to the indicated proteins. All Western blotting experiments were repeated twice, and representative images are shown.

Protease protection assay

TransIT-LT1 (Mirus) was used to transfect an expression construct coding for FLAG-LysMD3-HA into HeLa cells. 24 h post-transfection, cells were treated with 80 μM digitonin to permeabilize the plasma membrane. Samples were treated with the indicated concentration of proteinase K on ice, and protease activity was inhibited by the addition of phenylmethylsulfonyl fluoride prior to Western blot analysis with the indicated antibodies. Experiments were repeated twice, and representative blots are shown.

Immunofluorescence

MEFs or HeLa cells were seeded on coverslips, fixed in 4% methanol-free paraformaldehyde, permeabilized using 0.5% Triton X-100, and blocked in 1% BSA and 10% serum corresponding to the secondary antibody species. Cells were stained using the indicated primary and secondary antibodies and phalloidin AF594 or AF647 (Invitrogen). Coverslips were mounted using Prolong Gold Antifade reagent (Invitrogen). For determination of membrane orientation by immunofluorescence staining, TransIT-LT1 (Mirus) was used to transfect HeLa cells with the indicated LysMD3 constructs. Cells were fixed, blocked, and stained with an anti-GFP antibody prior to permeabilization using 0.5% Triton X-100, re-blocking, and re-staining for GFP where appropriate. Phalloidin-Alexa594 (Invitrogen) was used to visualize actin. Immunofluorescence images were acquired using a Zeiss LSM510 confocal microscope or a Zeiss LSM880 confocal laser-scanning microscope. Unless otherwise noted, three separate experiments were performed, and representative images are shown.

Table 2
Predesigned qPCR assays

Target	Assay
mLysMD3	Mm.PT.58.10100260
mLysMD4	Mm.PT.58.12179173
Adgrv1	Mm.PT.58.43743756
Polr3g	Mm.PT.58.10070464

qRT-PCR

RNA was extracted from tissues, and qRT-PCR was performed as described (61). RNA was extracted from tissues with TRIzol (Life Technologies, Inc.) or TRI Reagent (Sigma) according to the manufacturer's protocol. One μg of RNA was used as a template for random-primed cDNA synthesis with ImPromII reverse transcriptase (Promega). Transcripts were detected using predesigned TaqMan assays (IDT, Coralville, IA) listed in Table 2, and the absolute number of transcript copies was determined by comparison with target sequence-containing gBlocks (IDT) and normalized to actin (Table 1).

C. rodentium

Kanamycin-resistant *C. rodentium* strain DBS120 (62, 63) cultures in log-phase growth were pelleted and resuspended in PBS with 3% bicarbonate. Mice were infected with ~1e9 CFU intragastrically. Mice were subsequently weighed. Bacterial titers per stool pellet were determined by homogenizing a single stool pellet in 1 ml of PBS with 0.05% Triton X-100 using 1-mm silica beads (Biospec) on a mini-beadbeater 24 (Biospec) and plating serial dilutions on LB agar plates.

S. enterica serotype Typhimurium

S. enterica serotype Typhimurium SL1344 was used to inoculate streptomycin-pretreated mice, as described previously (18). Mice were fasted and pretreated with 200 μg of streptomycin 24 h before infection. On the day of infection, mice were fasted for 4 h, then gavaged with 1e8 CFU of SL1344 in PBS, and harvested in log-phase growth.

Histological preparation of tissues and colitis scoring

Colons and ceca were harvested and flushed with 10% neutral buffered formalin. Tissues were cut open, pinned flat, allowed to fix overnight at 4 °C, washed in 70% ethanol, and embedded in agar for processing. Sections were H&E-stained and scored for colitis severity using the following scoring system: 0, no acute inflammation; 1, acute inflammation in surface epithelium, lamina propria, or cryptitis; 2, crypt abscess; 3, acute inflammation present at muscularis mucosa or beyond; 4, ulcer or transmural inflammation. The extent of involved colon was also evaluated as an estimated percentage.

Listeria monocytogenes

L. monocytogenes strain EGD from a frozen glycerol stock was used to infect mice i.p. as described (64). *L. monocytogenes* experiments used B6 mice as controls and LysMD3-deficient mice were generated by intercrossing KO mice.

F. novicida

BMMo were differentiated in DMEM with 10% FBS and 20% macrophage colony-stimulating factor and infected with

F. novicida U112 and Δ*FPI* as described previously (65, 66). Cytotoxicity was measured using lactate dehydrogenase release (Promega), and type I IFN levels were measured using ISRE-L929 reporter cells (67).

M. tuberculosis

M. tuberculosis Erdman strain bacteria were used to infect mice by the aerosol route, as described previously (64, 68). Approximately 100 CFU of *M. tuberculosis* was inoculated using an Inhalation Exposure System (Glass-Col, Terre Haute, IN). At 0 or 24 HPI, 1–2 mice were sacrificed, and the number of CFU delivered per mouse were quantitated to determine infection efficiency. Tissue bacterial titers were determined by plating dilutions of lung and spleen homogenate on 7H10 agar plates.

B. abortus

Littermate-matched mice between the ages of 7 and 17 weeks were bred and housed at Washington University and shipped to UC Davis, where they were housed in microisolator cages with sterile bedding and irradiated feed in a biosafety level 3 laboratory. Mice were infected intraperitoneally (i.p.) with 1e6 CFU of *B. abortus* 2308. Spleens and livers were collected aseptically. Spleens and livers were homogenized, and serial dilutions of the homogenate were plated on tryptic soy agar for enumeration of CFUs.

L. pneumophila

Primary BMMo were infected with *L. pneumophila*, as described previously (30, 69). Lactate dehydrogenase release was quantitated using the Cytotox assay (Promega) as described previously (30).

Uropathogenic E. coli

Anesthetized female mice were transurethrally inoculated with 1e7 CFU UPEC strain UTI89. At 24 HPI, urine was collected for CFU enumeration and cytokine analysis; serum was collected for cytokine analysis, and bladder tissues were removed for inflammation scoring (70, 71). IL1β concentrations in the urine and serum were determined by ELISA (R&D Systems). A semiquantitative scoring system, with a scale of 0 (normal) to 5 (necrosis with full-thickness inflammatory infiltration), was used to evaluate bladder inflammation at 24 HPI (71). UTI89 infection of BMMo was performed as described (72). Briefly, macrophages were differentiated from whole bone marrow in DMEM containing 15% FBS and 30% L929 conditioned media. Cells were re-plated on day 8 and challenged with UTI89 on day 9 at an MOI of 0.1. Supernatant fluids were collected at the indicated time points, and IL1β concentration was determined as above.

C. trachomatis and S. flexneri

Infections of BMMo with *C. trachomatis* serovar L2 434/Bu at an MOI of 10 or *S. flexneri* serovar 2a WT strain 2457T at an MOI of 1 were performed in triplicate as described (73, 74), and supernatant fluids were collected for cytokine analysis using L929-ISRE fibroblasts to measure IFNβ levels (73). Sandwich ELISA was used to determine IL6 levels (BD Biosciences).

Serum-induced arthritis

Serum was isolated from K/BxN mice as described previously (34). Serum was injected intravenously (i.v.) into littermate-matched male mice, and morbidity and ankle swelling were determined at the indicated times post-serum transfer (75).

LPS treatments

Mice were injected i.p. with 20 mg/kg LPS purified by phenol extraction (Sigma L-2880). PECs were isolated by flushing the peritoneal cavity with 10 ml of ice-cold DMEM containing 10% FBS. Cells were counted, plated on 96-well tissue culture-treated plates, and incubated for 3 days. Cells were stimulated with 100 ng/ml LPS purified by ion-exchange chromatography (Sigma L4524) ± 16 h IFNγ pretreatment. Supernatant fluids were collected 6 h post-stimulation, and TNFα was quantitated by ELISA (BD Biosciences).

Influenza

8–12-Week-old mice were anesthetized and inoculated with 50 $TCID_{50}$ H1N1 influenza virus strain PR8 i.n., as described (76). Mice losing more than 30% of their initial body weight were sacrificed.

MHV68 ex vivo limiting dilution assay for reactivation from latency

MHV68 WUMS (ATCC VR1465) was used, and reactivation from latency was measured as described (36, 37, 77). Mice were infected with 1e6 PFU MHV68 i.p., and after 16 days, PECs or spleens were pooled from 3 to 5 mice, and serial dilutions of cells were plated on a MEF monolayer. After 3 weeks, wells were scored for cytopathic effect to detect reactivation. Data points represent the mean and standard error for three replicate experiments using three mice per genotype per experiment. MHV68 experiments used B6 mice as controls, and LysMD3-deficient mice were generated by intercrossing KO mice.

C. neoformans

C. neoformans strain KN99α was recovered from 15% glycerol stocks stored at −80 °C and maintained on YPD plates (1% yeast extract, 2% peptone, 2% dextrose, and 2% Bacto agar). A single colony was inoculated into YPD broth and grown for 16 h at 30 °C with shaking, collected by centrifugation, washed three times with sterile PBS, and counted on a Cellometer Auto M10 (Nexcelom Bioscience, Lawrence, MA). Female WT or LysMD3 KO littermate mice from the LysMD3 GT line were anesthetized by i.p. injection (of 150 μl of 2 mg/ml xylazine (VEDCO) and 10 mg/ml of ketaset (Fort Dodge Animal Health)) and i.n. inoculated with 5e4 CFU (verified by quantitative culture on YPD agar) in 50 μl of sterile PBS. Mice were euthanized when body weight fell below 80% of peak weight.

A. fumigatus

A. fumigatus CEA10 (CBS 144.89) was grown, and conidia were harvested similar to Ref. 78. Mice were infected i.n. with 1e7 conidia. Weight was monitored daily, and mice were sacrificed at 72 HPI. Lungs were lavaged with 1 ml of PBS with EDTA and fetal bovine serum. RBCs in the BAL were lysed, and

cell counts were performed. Cytospin preparations were analyzed by light microscopy to determine differential counts. Lungs were fixed, paraffin-embedded, and stained with hematoxylin and eosin for assessment of pathological changes. Hyphae were stained using Grocott methamine silver.

Antibiotic treatment of mice for 16S analysis

Female WT and KO mice were co-housed for 2 weeks, at a ratio of 2 WT and 2 KO mice per cage. After 2 weeks, mice were individually housed and were administered grape Kool-Aid ± a broad-spectrum antibiotic mixture in their drinking water (79) for another 2 weeks. The antibiotic mixture consisted of 1 g/liter ampicillin, 1 g/liter metronidazole, 1 g/liter neomycin, 0.5 g/liter vancomycin (Sigma) in 20 mg/ml grape Kool-Aid (Kraft Foods, Northfield, IL). After antibiotic treatment, stool pellets were collected for 16S analysis (79).

16S rRNA Illumina sequencing and analysis

Preparation of fecal pellets for 16S analysis was as described previously (79, 80). Briefly, DNA was phenol/chloroform-extracted and amplified in triplicate with Golay-barcoded primers specific for the V4 region of the 16S rRNA. Amplicons were pooled and purified with 0.6× Agencourt Ampure XP beads (Beckman-Coulter) prior to sequencing at the Center for Genome Sciences, Washington University School of Medicine, by the 2 × 250-bp protocol on the Illumina MiSeq platform. 16S rRNA gene sequences were resolved using dada2 (81). Taxonomy was assigned to resolved sequences according to the Greengenes database (version 13.8) (82). All subsequent analyses were performed using PhyloSeq (version 1.16.2) (83) to calculate richness, per sample Shannon diversity, and both weighted and unweighted UniFrac distances among samples (84). Differential abundance of bacterial taxa between experimental groups was determined using the PhyloSeq DESeq2 extension using the Wald significance test and a local fit type (version 1.6.3) (83, 85).

RNA-Seq

RNA from the distal ileum was purified; an Illumina sequencing library was generated, and libraries were sequenced (HiSeq platform), as described previously (37). Five to six mice were included in each group. DESeq2 was used to identify differentially expressed genes (85).

Sequencing data

RNA-seq and 16S sequencing data were deposited to the European nucleotide archive under the accession numbers PRJEB23707 and PRJEB25196, respectively.

Antigen presentation

Antigen presentation by BMMo was assessed as described (86, 87). BMMo were generated in 10% FBS and 10% CMG14–12 supernatant fluids (60) and infected with *L. monocytogenes* strain 10403S or pulsed with LLO peptide ± IFNγ priming. At 1 HPI, infected BMMo were washed with Dulbecco's PBS, and gentamycin was added. Splenic CD4 T cells isolated from LLO56tg mice (86), bearing a T cell receptor specific for LLO190-225, were isolated using a CD4-negative selection kit (Miltenyi Biotech, Bergisch Gladbach, Germany) and added to the macrophage cultures. After 24 h, cells were stained for CD4 (eFluor450, Clone RM4-5, eBioscience) and CD69 (PECy7, Clone H1.2F3, BioLegend) to evaluate activation status.

Author contributions—C. C. Y., M. T. B., D. W. L., J. E. D., G. K. A., C. A. M., and H. W. V. conceptualization; C. C. Y., G. Z., C. D., and S. A. H. data curation; C. C. Y. validation; C. C. Y., M. T. B., D. W. L., G. Z., T.-C. L., V. E. D.-O., J. P. H., J. M. K., E. L. S., C. R. H., R. A. I., S. P., K. M. S., C. W., A. V. M., E. C., and T. K. investigation; C. C. Y. visualization; C. C. Y., D. W. L., G. Z., C. D., T.-C. L., V. E. D.-O., J. P. H., J. M. K., E. L. S., C. R. H., R. A. I., S. P., K. M. S., C. W., S. H., A. V. M., E. C., T. K., M. N. S., I. U. M., P. M. A., D. M. M., M.C. D., T. L. D., R. M. T., C. L. S., and G. K. A. methodology; C. C. Y. writing-original draft; C. C. Y., M. T. B., D. W. L., G. Z., C. D., T.-C. L., V. E. D.-O., J. P. H., J. M. K., E. L. S., C. R. H., R. A. I., S. P., K. M. S., C. W., S. H., A. V. M., E. C., T. K., M. N. S., S. A. H., I. U. M., P. M. A., D. M. M., M.C. D., T. L. D., R. M. T., J. E. D., C. L. S., G. K. A., C. A. M., and H. W. V. writing-review and editing; M. T. B., D. W. L., M. N. S., S. A. H., I. U. M., P. M. A., D. M. M., M.C. D., T. L. D., R. M. T., C. L. S., G. K. A., C. A. M., and H. W. V. supervision; G. Z., C. D., T.-C. L., and S. A. H. formal analysis; C. D. software; S. H. resources; C. A. M. and H. W. V. project administration; H. W. V. funding acquisition.

Acknowledgments—We thank Darren Kreamalmeyer for assistance with animal husbandry; Andrea Bredemeyer, Barry Sleckman, and W. Tim Schaiff for technical assistance; and Broc T. McCune, Thomas Burke, and Daniel Portnoy for providing reagents. Experimental support was provided by the Genome Engineering Center of the Alvin J. Siteman Cancer Center, the Speed Congenics Facility, the Microinjection Core of the Rheumatic Diseases Core Center, and the Molecular Microbiology Imaging Facility at Washington University School of Medicine and Barnes-Jewish Hospital in St. Louis, MO. The Siteman Cancer Center is supported by National Institutes of Health Grant P30CA091842. The Rheumatic Diseases Core Center is supported by National Institutes of Health Grant P30AR048335.

References

1. Newton, K., and Dixit, V. M. (2012) Signaling in innate immunity and inflammation. *Cold Spring Harb. Perspect. Biol.* **4,** a006049 Medline
2. Eckert, C., Lecerf, M., Dubost, L., Arthur, M., and Mesnage, S. (2006) Functional analysis of AtlA, the major *N*-acetylglucosaminidase of *Enterococcus faecalis*. *J. Bacteriol.* **188,** 8513–8519 CrossRef Medline
3. Andre, G., Leenhouts, K., Hols, P., and Dufrêne, Y. F. (2008) Detection and localization of single LysM-peptidoglycan interactions. *J. Bacteriol.* **190,** 7079–7086 CrossRef Medline
4. Frankel, M. B., and Schneewind, O. (2012) Determinants of murein hydrolase targeting to cross-wall of *Staphylococcus aureus* peptidoglycan. *J. Biol. Chem.* **287,** 10460–10471 CrossRef Medline
5. Mesnage, S., Dellarole, M., Baxter, N. J., Rouget, J.-B., Dimitrov, J. D., Wang, N., Fujimoto, Y., Hounslow, A. M., Lacroix-Desmazes, S., Fukase, K., Foster, S. J., and Williamson, M. P. (2014) Molecular basis for bacterial peptidoglycan recognition by LysM domains. *Nat. Commun.* **5,** 4269 Medline
6. Wong, J. E., Midtgaard, S. R., Gysel, K., Thygesen, M. B., Sørensen, K. K., Jensen, K. J., Stougaard, J., Thirup, S., and Blaise, M. (2015) An intermolecular binding mechanism involving multiple LysM domains mediates carbohydrate recognition by an endopeptidase. *Acta Crystallogr. D Biol. Crystallogr.* 71, 592–605 CrossRef Medline

7. Caruso, R., Warner, N., Inohara, N., and Núñez, G. (2014) NOD1 and NOD2: signaling, host defense, and inflammatory disease. *Immunity* **41,** 898–908 CrossRef Medline
8. Djordjevic, M. A., Bezos, A., Susanti Marmuse, L., Driguez, H., Samain, E., Vauzeilles, B., Beau, J.-M., Kordbacheh, F., Rolfe, B. G., Schwörer, R., Daines, A. M., Gresshoff, P. M., and Parish, C. R. (2014) Lipo-chitin oligosaccharides, plant symbiosis signalling molecules that modulate mammalian angiogenesis *in vitro*. *PLoS ONE* **9,** e112635 CrossRef Medline
9. Wang, Z., Berkey, C. D., and Watnick, P. I. (2012) The *Drosophila* protein mustard tailors the innate immune response activated by the immune deficiency pathway. *J. Immunol.* **188,** 3993–4000 CrossRef Medline
10. Kelley, L. A., Mezulis, S., Yates, C. M., Wass, M. N., and Sternberg, M. J. (2015) The Phyre2 web portal for protein modeling, prediction and analysis. *Nat. Protoc.* **10,** 845–858 CrossRef Medline
11. Nakamura, N., Rabouille, C., Watson, R., Nilsson, T., Hui, N., Slusarewicz, P., Kreis, T. E., and Warren, G. (1995) Characterization of a cis-Golgi matrix protein, GM130. *J. Cell Biol.* **131,** 1715–1726 CrossRef Medline
12. Plutner, H., Davidson, H. W., Saraste, J., and Balch, W. E. (1992) Morphological analysis of protein transport from the ER to Golgi membranes in digitonin-permeabilized cells: role of the P58 containing compartment. *J. Cell Biol.* **119,** 1097–1116 CrossRef Medline
13. Cadwell, K., Liu, J. Y., Brown, S. L., Miyoshi, H., Loh, J., Lennerz, J. K., Kishi, C., Kc, W., Carrero, J. A., Hunt, S., Stone, C. D., Brunt, E. M., Xavier, R. J., Sleckman, B. P., Li, E., *et al.* (2008) A key role for autophagy and the autophagy gene Atg16l1 in mouse and human intestinal Paneth cells. *Nature* **456,** 259–263 CrossRef Medline
14. Pham, C. T., MacIvor, D. M., Hug, B. A., Heusel, J. W., and Ley, T. J. (1996) Long-range disruption of gene expression by a selectable marker cassette. *Proc. Natl. Acad. Sci. U.S.A.* **93,** 13090–13095 CrossRef Medline
15. Eckmann, L. (2006) Animal models of inflammatory bowel disease: lessons from enteric infections. *Ann. N.Y. Acad. Sci.* **1072,** 28–38 CrossRef Medline
16. Mundy, R., MacDonald, T. T., Dougan, G., Frankel, G., and Wiles, S. (2005) *Citrobacter rodentium* of mice and man. *Cell. Microbiol.* **7,** 1697–1706 CrossRef Medline
17. Vidal, S., Gros, P., and Skamene, E. (1995) Natural resistance to infection with intracellular parasites: molecular genetics identifies Nramp1 as the Bcg/Ity/Lsh locus. *J. Leukocyte Biol.* **58,** 382–390 CrossRef Medline
18. Barthel, M., Hapfelmeier, S., Quintanilla-Martínez, L., Kremer, M., Rohde, M., Hogardt, M., Pfeffer, K., Rüssmann, H., and Hardt, W.-D. (2003) Pretreatment of mice with streptomycin provides a *Salmonella enterica* serovar Typhimurium colitis model that allows analysis of both pathogen and host. *Infect. Immun.* **71,** 2839–2858 CrossRef Medline
19. Pamer, E. G. (2004) Immune responses to *Listeria monocytogenes*. *Nat. Rev. Immunol.* **4,** 812–823 CrossRef Medline
20. Oyston, P. C., Sjostedt, A., and Titball, R. W. (2004) Tularaemia: bioterrorism defence renews interest in *Francisella tularensis*. *Nat. Rev. Microbiol.* **2,** 967–978 CrossRef Medline
21. Weiss, D. S., Brotcke, A., Henry, T., Margolis, J. J., Chan, K., and Monack, D. M. (2007) *In vivo* negative selection screen identifies genes required for *Francisella* virulence. *Proc. Natl. Acad. Sci. U.S.A.* **104,** 6037–6042 CrossRef Medline
22. Frieden, T. R., Sterling, T. R., Munsiff, S. S., Watt, C. J., and Dye, C. (2003) Tuberculosis. *Lancet* **362,** 887–899 Medline
23. Zumla, A., Raviglione, M., Hafner, R., and von Reyn, C. F. (2013) Tuberculosis. *N. Engl. J. Med.* **368,** 745–755 CrossRef Medline
24. O'Garra, A., Redford, P. S., McNab, F. W., Bloom, C. I., Wilkinson, R. J., and Berry, M. P. (2013) The immune response in tuberculosis. *Annu. Rev. Immunol.* **31,** 475–527 CrossRef Medline
25. Flynn, J. L., and Chan, J. (2001) Immunology of tuberculosis. *Annu. Rev. Immunol.* **19,** 93–129 CrossRef Medline
26. Philips, J. A., and Ernst, J. D. (2012) Tuberculosis pathogenesis and immunity. *Annu. Rev. Pathol.* **7,** 353–384 CrossRef Medline
27. Pappas, G., Akritidis, N., Bosilkovski, M., and Tsianos, E. (2005) Brucellosis. *N. Engl. J. Med.* **352,** 2325–2336 CrossRef Medline
28. Byndloss, M. X., and Tsolis, R. M. (2016) *Brucella* spp. virulence factors and immunity. *Annu. Rev. Anim. Biosci.* **4,** 111–127 CrossRef Medline
29. Fields, B. S., Benson, R. F., and Besser, R. E. (2002) Legionella and Legionnaires' disease: 25 years of investigation. *Clin. Microbiol. Rev.* **15,** 506–526 CrossRef Medline
30. Ren, T., Zamboni, D. S., Roy, C. R., Dietrich, W. F., and Vance, R. E. (2006) Flagellin-deficient *Legionella* mutants evade caspase-1- and Naip5-mediated macrophage immunity. *PLoS Pathog.* **2,** e18 CrossRef Medline
31. Vance, R. E. (2010) Immunology taught by bacteria. *J. Clin. Immunol.* **30,** 507–511 CrossRef Medline
32. Terlizzi, M. E., Gribaudo, G., and Maffei, M. E. (2017) UroPathogenic *Escherichia coli* (UPEC) infections: virulence factors, bladder responses, antibiotic, and non-antibiotic antimicrobial strategies. *Front. Microbiol.* **8,** 1566 CrossRef Medline
33. Heng, T. S., Painter, M. W., and Immunological Genome Project Consortium. (2008) The Immunological Genome Project: networks of gene expression in immune cells. *Nat. Immunol.* **9,** 1091–1094 CrossRef Medline
34. Wipke, B. T., and Allen, P. M. (2001) Essential role of neutrophils in the initiation and progression of a murine model of rheumatoid arthritis. *J. Immunol.* **167,** 1601–1608 CrossRef Medline
35. Sadik, C. D., Kim, N. D., Iwakura, Y., and Luster, A. D. (2012) Neutrophils orchestrate their own recruitment in murine arthritis through C5aR and FcγR signaling. *Proc. Natl. Acad. Sci. U.S.A.* **109,** E3177–E3185 CrossRef Medline
36. Tibbetts, S. A., Loh, J., Van Berkel, V., McClellan, J. S., Jacoby, M. A., Kapadia, S. B., Speck, S. H., and Virgin, H. W., 4th. (2003) Establishment and maintenance of gammaherpesvirus latency are independent of infective dose and route of infection. *J. Virol.* **77,** 7696–7701 CrossRef Medline
37. Park, S., Buck, M. D., Desai, C., Zhang, X., Loginicheva, E., Martinez, J., Freeman, M. L., Saitoh, T., Akira, S., Guan, J.-L., He, Y.-W., Blackman, M. A., Handley, S. A., Levine, B., Green, D. R., *et al.* (2016) Autophagy genes enhance murine gammaherpesvirus 68 reactivation from latency by preventing virus-induced systemic inflammation. *Cell Host Microbe* **19,** 91–101 CrossRef Medline
38. Tanaka, K., Nguyen, C. T., Liang, Y., Cao, Y., and Stacey, G. (2013) Role of LysM receptors in chitin-triggered plant innate immunity. *Plant Signal. Behav.* **8,** e22598 Medline
39. Wu, C., Orozco, C., Boyer, J., Leglise, M., Goodale, J., Batalov, S., Hodge, C. L., Haase, J., Janes, J., Huss, J. W., 3rd., and Su, A. I. (2009) BioGPS: an extensible and customizable portal for querying and organizing gene annotation resources. *Genome Biol.* **10,** R130 CrossRef Medline
40. Mombaerts, P., Iacomini, J., Johnson, R. S., Herrup, K., Tonegawa, S., and Papaioannou, V. E. (1992) RAG-1-deficient mice have no mature B and T lymphocytes. *Cell* **68,** 869–877 CrossRef Medline
41. Lattin, J. E., Schroder, K., Su, A. I., Walker, J. R., Zhang, J., Wiltshire, T., Saijo, K., Glass, C. K., Hume, D. A., Kellie, S., and Sweet, M. J. (2008) Expression analysis of G protein-coupled receptors in mouse macrophages. *Immunome Res.* **4,** 5 CrossRef Medline
42. Su, A. I., Wiltshire, T., Batalov, S., Lapp, H., Ching, K. A., Block, D., Zhang, J., Soden, R., Hayakawa, M., Kreiman, G., Cooke, M. P., Walker, J. R., and Hogenesch, J. B. (2004) A gene atlas of the mouse and human protein-encoding transcriptomes. *Proc. Natl. Acad. Sci. U.S.A.* **101,** 6062–6067 CrossRef Medline
43. Weinberg, S. E., Sena, L. A., and Chandel, N. S. (2015) Mitochondria in the regulation of innate and adaptive immunity. *Immunity* **42,** 406–417 CrossRef Medline
44. Cho, K.-O., Kim, G.-W., and Lee, O.-K. (2011) *Wolbachia* bacteria reside in host Golgi-related vesicles whose position is regulated by polarity proteins. *PLoS ONE* **6,** e22703 CrossRef Medline
45. Hilbi, H., and Haas, A. (2012) Secretive bacterial pathogens and the secretory pathway. *Traffic* **13,** 1187–1197 CrossRef Medline
46. Dolat, L., and Valdivia, R. H. (2017) Bacterial subversion of COG-dependent membrane traffic. *Trends Cell Biol.* **27,** 877–878 CrossRef Medline
47. Medzhitov, R., Preston-Hurlburt, P., and Janeway, C. A. (1997) A human homologue of the *Drosophila* Toll protein signals activation of adaptive immunity. *Nature* **388,** 394–397 CrossRef Medline
48. Lemaitre, B., Nicolas, E., Michaut, L., Reichhart, J. M., and Hoffmann, J. A. (1996) The dorsoventral regulatory gene cassette spätzle/Toll/cactus controls the potent antifungal response in *Drosophila* adults. *Cell* **86,** 973–983 CrossRef Medline

49. Dziarski, R., and Gupta, D. (2010) Review: Mammalian peptidoglycan recognition proteins (PGRPs) in innate immunity. *Innate Immun.* **16,** 168–174 CrossRef Medline
50. Xu, M., Wang, Z., and Locksley, R. M. (2004) Innate immune responses in peptidoglycan recognition protein L-deficient mice. *Mol. Cell. Biol.* **24,** 7949–7957 CrossRef Medline
51. Anderson, K. V., Jürgens, G., and Nüsslein-Volhard, C. (1985) Establishment of dorsal-ventral polarity in the *Drosophila* embryo: genetic studies on the role of the Toll gene product. *Cell* **42,** 779–789 CrossRef Medline
52. Lemaitre, B., and Hoffmann, J. (2007) The host defense of *Drosophila melanogaster*. *Annu. Rev. Immunol.* **25,** 697–743 CrossRef Medline
53. Laroche, F. J., Tulotta, C., Lamers, G. E., Meijer, A. H., Yang, P., Verbeek, F. J., Blaise, M., Stougaard, J., and Spaink, H. P. (2013) The embryonic expression patterns of zebrafish genes encoding LysM-domains. *Gene Expr. Patterns* **13,** 212–224 CrossRef Medline
54. Parikh, B. A., Beckman, D. L., Patel, S. J., White, J. M., and Yokoyama, W. M. (2015) Detailed phenotypic and molecular analyses of genetically modified mice generated by CRISPR-Cas9-mediated editing. *PLoS ONE* **10,** e0116484 CrossRef Medline
55. Selleck, E. M., Orchard, R. C., Lassen, K. G., Beatty, W. L., Xavier, R. J., Levine, B., Virgin, H. W., and Sibley, L. D. (2015) A noncanonical autophagy pathway restricts *Toxoplasma gondii* growth in a strain-specific manner in IFN-γ-activated human cells. *mBio.* **6,** e01157-15 Medline
56. Lee, S., Salwinski, L., Zhang, C., Chu, D., Sampankanpanich, C., Reyes, N. A., Vangeloff, A., Xing, F., Li, X., Wu, T.-T., Sahasrabudhe, S., Deng, H., Lacount, D. J., and Sun, R. (2011) An integrated approach to elucidate the intra-viral and viral-cellular protein interaction networks of a gammaherpesvirus. *PLoS Pathog.* **7,** e1002297 CrossRef Medline
57. Tamura, K., Stecher, G., Peterson, D., Filipski, A., and Kumar, S. (2013) MEGA6: molecular evolutionary genetics analysis version 6.0. *Mol. Biol. Evol.* **30,** 2725–2729 CrossRef Medline
58. Page, R. D. (1996) TreeView: an application to display phylogenetic trees on personal computers. *Comput. Appl. Biosci.* **12,** 357–358 Medline
59. Hwang, S., Maloney, N. S., Bruinsma, M. W., Goel, G., Duan, E., Zhang, L., Shrestha, B., Diamond, M. S., Dani, A., Sosnovtsev, S. V., Green, K. Y., Lopez-Otín, C., Xavier, R. J., Thackray, L. B., and Virgin, H. W. (2012) Nondegradative role of Atg5-Atg12/ Atg16L1 autophagy protein complex in antiviral activity of interferon γ. *Cell Host Microbe* **11,** 397–409 CrossRef Medline
60. Takeshita, S., Kaji, K., and Kudo, A. (2000) Identification and characterization of the new osteoclast progenitor with macrophage phenotypes being able to differentiate into mature osteoclasts. *J. Bone Miner. Res.* **15,** 1477–1488 CrossRef Medline
61. Yokoyama, C. C., Loh, J., Zhao, G., Stappenbeck, T. S., Wang, D., Huang, H. V., Virgin, H. W., and Thackray, L. B. (2012) Adaptive immunity restricts replication of novel murine astroviruses. *J. Virol.* **86,** 12262–12270 CrossRef Medline
62. Schauer, D. B., and Falkow, S. (1993) The eae gene of *Citrobacter freundii* biotype 4280 is necessary for colonization in transmissible murine colonic hyperplasia. *Infect. Immun.* **61,** 4654–4661 Medline
63. Kim, Y.-G., Kamada, N., Shaw, M. H., Warner, N., Chen, G. Y., Franchi, L., and Núñez, G. (2011) The Nod2 sensor promotes intestinal pathogen eradication via the chemokine CCL2-dependent recruitment of inflammatory monocytes. *Immunity* **34,** 769–780 CrossRef Medline
64. MacDuff, D. A., Reese, T. A., Kimmey, J. M., Weiss, L. A., Song, C., Zhang, X., Kambal, A., Duan, E., Carrero, J. A., Boisson, B., Laplantine, E., Israel, A., Picard, C., Colonna, M., Edelson, B. T., Sibley, L. D., Stallings, C. L., Casanova, J.-L., Iwai, K., and Virgin, H. W. (2015) Phenotypic complementation of genetic immunodeficiency by chronic herpesvirus infection. *Elife* **4,** e04494 CrossRef Medline
65. Peng, K., Broz, P., Jones, J., Joubert, L.-M., and Monack, D. (2011) Elevated AIM2-mediated pyroptosis triggered by hypercytotoxic *Francisella* mutant strains is attributed to increased intracellular bacteriolysis. *Cell. Microbiol.* **13,** 1586–1600 CrossRef Medline
66. Storek, K. M., Gertsvolf, N. A., Ohlson, M. B., and Monack, D. M. (2015) cGAS and Ifi204 cooperate to produce type I IFNs in response to *Francisella* infection. *J. Immunol.* **194,** 3236–3245 CrossRef Medline
67. Jiang, Z., Georgel, P., Du, X., Shamel, L., Sovath, S., Mudd, S., Huber, M., Kalis, C., Keck, S., Galanos, C., Freudenberg, M., and Beutler, B. (2005) CD14 is required for MyD88-independent LPS signaling. *Nat. Immunol.* **6,** 565–570 CrossRef Medline
68. Kimmey, J. M., Huynh, J. P., Weiss, L. A., Park, S., Kambal, A., Debnath, J., Virgin, H. W., and Stallings, C. L. (2015) Unique role for ATG5 in neutrophil-mediated immunopathology during *M. tuberculosis* infection. *Nature* **528,** 565–569 CrossRef Medline
69. Wright, E. K., Goodart, S. A., Growney, J. D., Hadinoto, V., Endrizzi, M. G., Long, E. M., Sadigh, K., Abney, A. L., Bernstein-Hanley, I., and Dietrich, W. F. (2003) Naip5 affects host susceptibility to the intracellular pathogen *Legionella* pneumophila. *Curr. Biol.* **13,** 27–36 CrossRef Medline
70. Mysorekar, I. U., and Hultgren, S. J. (2006) Mechanisms of uropathogenic *Escherichia coli* persistence and eradication from the urinary tract. *Proc. Natl. Acad. Sci. U.S.A.* **103,** 14170–14175 CrossRef Medline
71. Stemler, K. M., Crock, L. W., Lai, H. H., Mills, J. C., Gereau, R. W., 4th., and Mysorekar, I. U. (2013) Protamine sulfate induced bladder injury protects from distention induced bladder pain. *J. Urol.* **189,** 343–351 CrossRef Medline
72. Symington, J. W., Wang, C., Twentyman, J., Owusu-Boaitey, N., Schwendener, R., Núñez, G., Schilling, J. D., and Mysorekar, I. U. (2015) ATG16L1 deficiency in macrophages drives clearance of uropathogenic *E. coli* in an IL-1β-dependent manner. *Mucosal Immunol.* **8,** 1388–1399 CrossRef Medline
73. Jehl, S. P., Nogueira, C. V., Zhang, X., and Starnbach, M. N. (2012) IFNγ inhibits the cytosolic replication of *Shigella flexneri* via the cytoplasmic RNA sensor RIG-I. *PLoS Pathog.* **8,** e1002809 CrossRef Medline
74. Gondek, D. C., Olive, A. J., Stary, G., and Starnbach, M. N. (2012) $CD4^+$ T cells are necessary and sufficient to confer protection against *Chlamydia trachomatis* infection in the murine upper genital tract. *J. Immunol.* **189,** 2441–2449 CrossRef Medline
75. Monach, P., Hattori, K., Huang, H., Hyatt, E., Morse, J., Nguyen, L., Ortiz-Lopez, A., Wu, H.-J., Mathis, D., and Benoist, C. (2007) The K/BxN mouse model of inflammatory arthritis, theory and practice. *Methods Mol. Med.* **136,** 269–282 CrossRef Medline
76. Lu, Q., Yokoyama, C. C., Williams, J. W., Baldridge, M. T., Jin, X., DesRochers, B., Bricker, T., Wilen, C. B., Bagaitkar, J., Loginicheva, E., Sergushichev, A., Kreamalmeyer, D., Keller, B. C., Zhao, Y., Kambal, A., *et al.* (2016) Homeostatic control of innate lung inflammation by Vici syndrome gene Epg5 and additional autophagy genes promotes influenza pathogenesis. *Cell Host Microbe* **19,** 102–113 CrossRef Medline
77. Weck, K. E., Barkon, M. L., Yoo, L. I., Speck, S. H., Virgin, H. W. (1996) Mature B cells are required for acute splenic infection, but not for establishment of latency, by murine gammaherpesvirus 68. *J. Virol.* **70,** 6775–6780 Medline
78. Morgenstern, D. E., Gifford, M. A., Li, L. L., Doerschuk, C. M., and Dinauer, M. C. (1997) Absence of respiratory burst in X-linked chronic granulomatous disease mice leads to abnormalities in both host defense and inflammatory response to *Aspergillus fumigatus*. *J. Exp. Med.* **185,** 207–218 CrossRef Medline
79. Baldridge, M. T., Nice, T. J., McCune, B. T., Yokoyama, C. C., Kambal, A., Wheadon, M., Diamond, M. S., Ivanova, Y., Artyomov, M., and Virgin, H. W. (2015) Commensal microbes and interferon-λ determine persistence of enteric murine norovirus infection. *Science* **347,** 266–269 CrossRef Medline
80. Caporaso, J. G., Lauber, C. L., Walters, W. A., Berg-Lyons, D., Lozupone, C. A., Turnbaugh, P. J., Fierer, N., and Knight, R. (2011) Global patterns of 16S rRNA diversity at a depth of millions of sequences per sample. *Proc. Natl. Acad. Sci. U.S.A.* **108,** Suppl. 1, 4516–4522 CrossRef Medline
81. Callahan, B. J., McMurdie, P. J., Rosen, M. J., Han, A. W., Johnson, A. J., and Holmes, S. P. (2016) DADA2: High-resolution sample inference from Illumina amplicon data. *Nat. Methods* **13,** 581–583 CrossRef Medline
82. McDonald, D., Price, M. N., Goodrich, J., Nawrocki, E. P., DeSantis, T. Z., Probst, A., Andersen, G. L., Knight, R., and Hugenholtz, P. (2012) An improved Greengenes taxonomy with explicit ranks for ecological and evolutionary analyses of bacteria and archaea. *ISME J.* **6,** 610–618 CrossRef Medline

83. McMurdie, P. J., and Holmes, S. (2012) Phyloseq: A bioconductor package for handling and analysis of high-throughput phylogenetic sequence data. *Pac. Symp. Biocomput.* **2012,** 235–246 Medline
84. Lozupone, C., and Knight, R. (2005) UniFrac: a new phylogenetic method for comparing microbial communities. *Appl. Environ. Microbiol.* **71,** 8228–8235 CrossRef Medline
85. Love, M. I., Huber, W., and Anders, S. (2014) Moderated estimation of fold change and dispersion for RNA-seq data with DESeq2. *Genome Biol.* **15,** 550 CrossRef Medline
86. Weber, K. S., Li, Q. J., Persaud, S. P., Campbell, J. D., Davis, M. M., and Allen, P. M. (2012) Distinct $CD4^+$ helper T cells involved in primary and secondary responses to infection. *Proc. Natl. Acad. Sci. U.S.A.* **109,** 9511–9516 CrossRef Medline
87. Redmann, V., Lamb, C. A., Hwang, S., Orchard, R. C., Kim, S., Razi, M., Milam, A., Park, S., Yokoyama, C. C., Kambal, A., Kreamalmeyer, D., Bosch, M. K., Xiao, M., Green, K., Kim, J., *et al.* (2016) Clec16a is critical for autolysosome function and Purkinje cell survival. *Sci. Rep.* **6,** 23326 CrossRef Medline

LysMD3 is a type II membrane protein without an *in vivo* role in the response to a range of pathogens

Christine C. Yokoyama, Megan T. Baldridge, Daisy W. Leung, Guoyan Zhao, Chandni Desai, Ta-Chiang Liu, Vladimir E. Diaz-Ochoa, Jeremy P. Huynh, Jacqueline M. Kimmey, Erica L. Sennott, Camaron R. Hole, Rachel A. Idol, Sunmin Park, Kelly M. Storek, Caihong Wang, Seungmin Hwang, Ashley Viehmann Milam, Eric Chen, Tobias Kerrinnes, Michael N. Starnbach, Scott A. Handley, Indira U. Mysorekar, Paul M. Allen, Denise M. Monack, Mary C. Dinauer, Tamara L. Doering, Renee M. Tsolis, Jonathan E. Dworkin, Christina L. Stallings, Gaya K. Amarasinghe, Craig A. Micchelli and Herbert W. Virgin

J. Biol. Chem. 2018, 293:6022-6038.
doi: 10.1074/jbc.RA117.001246 originally published online March 1, 2018